Optimal linker length for small molecule PROTACs that selectively target p38α and p38β for degradation

Craig Donoghue[1,†], Monica Cubillos-Rojas[1,†], Nuria Gutierrez-Prat[1,†], Carolina Sanchez-Zarzalejo[1], Xavier Verdaguer[1,2], Antoni Riera[1,2,*] and Angel R. Nebreda[1,3,*]

[1]Institute for Research in Biomedicine (IRB Barcelona), The Barcelona Institute of Science and Technology, Baldiri Reixac 10, 08028 Barcelona, Spain
[2]Dept. Química Inorgànica i Orgànica, Universitat de Barcelona, Martí i Franquès 1, 08028 Barcelona, Spain.
[3]ICREA, Pg. Lluís Companys 23, 08010 Barcelona, Spain

[†] These authors contributed equally
[*]Correspondence: angel.nebreda@irbbarcelona.org, phone: +34-934031379, antoni.riera@irbbarcelona.org, phone: +34-934037093

ABSTRACT

We report the design of hetero-bifunctional small molecules that selectively target p38α and p38β for degradation. These proteolysis targeted chimeras (PROTACs) are based on an ATP competitive inhibitor of p38α and p38β, which is linked to thalidomide analogues to recruit the Cereblon E3 ubiquitin ligase complex. Compound synthesis was facilitated by the use of a copper catalyzed "click" reaction. We show that optimization of the linker length and composition is crucial for the degradation-inducing activity of these PROTACs. We provide evidence that these chemical compounds can induce degradation of p38α and p38β but no other related kinases at nanomolar concentrations in several mammalian cell lines. Accordingly, the PROTACs inhibit stress and cytokine-induced p38α signaling. Our compounds contribute to understanding the development of PROTACs, and provide a useful tool to investigate functions of the p38 MAPK pathway and its involvement in diseases.

KEYWORDS: Azide-alkyne click reaction, Cereblon, p38 MAPK, PROTAC linker optimization, Protein degradation, Thalidomide derivative

1. Introduction

The p38 mitogen-activated protein kinase (MAPK) family comprises four members, p38α, p38β, p38γ and p38δ, with p38α being ubiquitously expressed and the most abundant family member in almost all cell types. Many functions that are generally ascribed to p38 MAPKs actually refer to p38α [1]. However, there is evidence that p38β may have redundant functions with p38α, although it is usually expressed at lower levels [2]. In contrast, p38γ and p38δ have more restricted expression patterns and perform different functions [1]. Extensive evidence indicates that p38α is activated in response to stress and can regulate many cellular processes by controlling the phosphorylation of a large variety of substrates [3]. Consequently, dysregulated p38α activity has been associated with several human pathologies including inflammatory diseases and cancer. This has made p38α an attractive therapeutic target and many small molecules of different structures have been developed by pharmaceutical companies to inhibit the activity of this kinase [4]. It has also been reported that p38α might regulate particular functions in a kinase-independent manner [5, 6], supporting the need to develop novel therapeutic approaches.

The functions of p38α are highly dependent on both the cell type and the context. For example, during tumorigenesis, p38α usually functions as a tumor suppressor in normal epithelial cells, whereas in malignant cells p38α tends to support tumor development [7]. Considering that p38α can also play diverse roles in cells of the tumor microenvironment [8, 9], it is clear that the contribution of p38α to tumor development is not straightforward. Nevertheless, the available information suggests potential therapeutic opportunities in several tumor types via intervention of the p38α pathway, especially when this is combined with chemotherapeutic drugs [10]. However, currently available p38α inhibitors have not shown the expected efficacy in clinical trials and there is a need to develop improved therapies that target p38α signaling. A greater understanding of how p38α downregulation or inhibition affects cellular functions would aid in therapeutically targeting this pathway.

Proteolysis targeting chimeras, referred to as PROTACs, are bifunctional compounds that hijack ubiquitinating enzymes to induce the degradation of a target protein by the ubiquitin proteasome pathway. Structurally, PROTACs consist of one end that binds to the target protein covalently linked to an E3 ubiquitin ligase ligand. Several ligand-like small molecules have been reported to engage E3 ligases and cause the poly-ubiquitination of target proteins, including peptide recognition fragments and thalidomide analogues [11]. By bringing the target protein and the E3 ligase in close proximity to each other, the target

protein can be poly-ubiquitinated and then degraded by the proteasome [12]. PROTAC-induced protein degradation normally results in a superior level of selectivity, as ubiquitination is dependent upon formation of a stable ternary complex and highly sensitive to linker distance and geometries. Therefore, not all off-target interactions would result in protein degradation [13]. To date, many targets have been reported using small-molecule, polypeptide or hydrophobic tagging degraders to achieve promising pre-clinical results [14, 15].

Here, we present the design of chemical compounds that achieve the selective degradation of p38α and p38β in mammalian cells at nanomolar concentrations. These compounds will assist in uncovering further functions of the p38 MAPK pathway that are not easily addressed by conventional inhibitors, and could aid in the development of improved therapies.

2. Results

2.1. Generation of PROTACs that induce p38α degradation.

For the warhead, we selected the small molecular weight compound PH-797804, an ATP competitor that potently inhibits p38α in various cellular models [10, 16-18]. PH-797804 possesses a methyl amide moiety amenable for linker attachment that resides in the solvent exposed region, extending out from the ATP binding site when bound to p38α. Furthermore, modifying this position was unlikely to interfere with the key interactions that determine the inhibitor activity and selectivity [19] (Fig. 1a). We reasoned that this location would be best for the attachment of the linker, directing the E3 ubiquitin ligase away from the p38α´s active site and allowing heterodimerization of p38α and the E3 ligase. We used analogues of thalidomide to recruit Cereblon (CRBN) E3 ligases and cause p38α ubiquitination [20]. Thalidomide analogues can be synthesized easily from commercially available starting materials (Fig. 1b). A structurally unrelated PROTAC (SJFα) has been recently reported to induce p38α degradation, featuring the c-Met kinase inhibitor foretinib as a warhead to bind p38α, linked to a ligand to engage the von Hippel-Lindau E3 ligase [21]. We opted to construct our PROTAC from basic and economic chemical starting materials and to utilize a warhead that would selectively target p38α, in order to reduce the possibility of inducing the degradation of other kinases [19].

Once the structural components at either side of the p38α PROTAC were decided, we focused on the optimization of the linker length and composition, as well as the type of attachment to the warhead and ligase ligand. An initial collection of compounds (**NR-1a-c** and **NR-2a-b**) with varying linker lengths and attachment points was synthesized (Supporting Information) and tested to monitor their ability to induce p38α degradation in mammalian cells (Table 1). We chose the breast cancer cell lines BBL358 and T47D as p38α has been shown to play a key role in breast tumors and we have previously reported the anti-proliferative effect of p38α inhibition in breast cancer cells [10]. We found that compounds with a linker length of 8 atomic units or less did not induce degradation of p38α in the cell lines tested, presumably because the PROTACs were not long enough to allow sufficient space for productive interaction between p38α and CRBN. However, PROTAC **NR-1c** with a linker of 20 atoms efficiently induced p38α degradation in BBL358 cells and, to a lesser extent, in T47D cells (Table 1 and Fig. S1a).

To further explore the influence of the linker length and composition on the PROTAC's activity, we developed a practical synthesis of PROTAC molecules aided by a "click" reaction [22]. The PH-797804 derivatives containing a terminal alkyne **8a-c** were formed via peptide coupling of carboxylic acid intermediate **1** with corresponding alkyne amines (Scheme 1). The thalidomide components containing an azide **9a-b** were formed from 4-fluorothalidomide (**2**) via S_NAr followed by standard derivatization (Fig 2 and Supplementary Information). Compound **15d** was prepared from carboxylic acid **4.** Finally, the azide and alkyne components were "clicked" together via a copper catalyzed Huisgen cycloaddition reaction to form 1,2,3-triazole containing PROTACs **NR-3a-c** and **NR-4** (Fig 2).

Our strategy introduced triazole and amide moieties that reduced linker flexibility and also facilitated the synthesis of compounds with longer linkers. Another click platform has been recently published for degradation of the bromodomain and extraterminal domain-4 (BRD4) [23]. Moreover, positive interaction of heteroatoms in the linker with amino acid residues on the protein's surfaces has been reported to enhance the protein-protein interaction induced by PROTACs [24]. Therefore, we synthesized compounds **NR-3-4** (Supporting Information) and tested their ability to induce p38α degradation (Table 2). Of the **NR-3** compounds with an amine linker at position 4' of thalidomide, only **NR-3c** showed clear activity in both BBL358 and T47D cells. It is worth noting that the connection to thalidomide strongly influenced the PROTAC's ability to induce p38α degradation, since PROTACs **NR-**

3c and **NR-4** featured the same linker with a different connection and showed different activities (Table 2 and Supporting Information Fig. S1b). As expected, blocking the imide of the piperidindione with an ortho-nitrobenzylgroup (**NR-3d**) strongly reduced the activity of the compound.

To further test the influence of the attachment mode, we synthesized compounds **NR-5a-b** and **NR-6a-b** since it has been reported that the potency of PROTACs targeting BRD4 was improved by replacing the 4' NH group of the thalidomide analogue with a 4' methylene group and removing one carbonyl from the indoline moiety [25, 26]. The synthesis of **NR-5** and **NR-6** started from thalidomide and deoxothalidomide derivatives **13a-d** with an aminoalkyl sidechain [26]. The azido group was incorporated as an amide with 4-azidobutanoic acid (**11)**. The click reaction of azides **14a-d** with the acetylenic derivative **8a** afforded the desired PROTACs **NR-5** and **NR-6** (Fig 3) as expected. Thus, we examined the effect of medium length methylene linkers on the ability of PROTACs to induce p38α degradation with and without the pthalimide carbonyl. We found that **NR-6a** was very potent at inducing p38α degradation in both BBL358 and T47D cells (Table 3 and Supporting Information Fig. S1b).

We, then synthesized a small series of *N*-linked PROTACs **NR-7a-h** starting from amines **3a-c** which were prepared from 4-fluorothalidomide **2** by SNAr. The azido functionality was introduced again by amide formation with 4-azidobutanoic acid (**11)**. This family of compounds was generated making minor adjustments to the length at either side of the triazole and amide moieties using alkyl fragments of 2-4 carbons in length. These PROTACs were then tested in cancer cell lines (Table 3). We found that a linker length of 15-17 atoms was optimum for the degradation of p38α in both BBL358 cells and T47D cells, whereas PROTACs bearing linkers shorter than 15 atoms poorly induced p38α degradation (Table 3 and Supporting Information Fig. S1c).

Out of the 24 compounds that were synthesized following the design mentioned above, we selected five compounds (**NR-6a, NR-7f-i**) that at 10 μM efficiently induced p38α downregulation in both BBL358 and T47D cancer cells (Supporting Information Fig. S1). To compare the efficacy of p38α downregulation induced by these five PROTACs, we treated T47D cells with different concentrations of the compounds (Supporting Information Fig. S2). Based on these results, we selected the PROTACs **NR-6a** and **NR-7h** (Fig. 4a) for further characterization, as both of them efficiently induced p38α downregulation at nanomolar concentrations. We calculated the concentrations of **NR-7h** and **NR-6a** required to

induce 50% of p38α degradation (DC_{50}) and obtained values between 3 and 27 nM in two different cancer cell lines (Fig. 4b).

In summary, we synthesized and tested 24 compounds. We have not investigated other inhibitors for p38 as warheads, as PH-79780 gave superb potencies in the nanomolar range. Neither have we investigated induction of other E3 ligases, e.g. VHL, which has been investigated thoroughly by Crews et al. Therefore, our efforts were concentrated on linker composition and length. From our small structure-activity study (SAR) we could conclude that a minimum linker length of 15 atoms is necessary to have good activity. The linker can be as long as 20 atoms but the optimum size is 16-17. The connection to the indoline moiety is a crucial aspect, with the alkyl and amino alkyl substituent at the 4'-position giving the best activities. Compounds derived from carboxylic acid **4** did not lead to degradation of p38α.

Next, we synthesized the analogs **NR-7h*** and **NR-6a***, featuring an additional methyl group to block the NH functionality of the thalidomide group (Supporting Information Fig. S3), which has been shown to prevent binding to CRBN [25] and therefore prevent ubiquitination of the target protein. These modifications impaired the ability of the compounds to induce the degradation of p38α in two different cells lines (Fig. 5), supporting the implication of CRBN-mediated ubiquitination.

To try to improve the aqueous solubility of **NR-7h**, compounds **NR-7i** and **NR-7j** were synthesized, featuring an additional branched functionality on the linker, a *tert*-butyl carbamate or a hydrochloride amine salt respectively (Fig. 6). Whereas the amine salt group of **NR-7j** improved aqueous solubility, it did not induce degradation of p38α in cells, potentially affecting the interaction between p38α and the E3 ligase or diminishing cell permeability. However, **NR-7i** induced degradation of p38α to a similar level as the parental **NR-7h**, which although did not improve aqueous solubility, demonstrated the potential for this position to serve as a derivatization point to improve the pharmacokinetic properties or for conjugation for directed delivery.

2.2 PROTACs target p38α and p38β for degradation.

It has been reported that PH-797804 potently inhibits p38α but it can also inhibit p38β at higher concentrations, whereas it has no inhibitory effect on other MAPKs, including the structurally related p38γ and p38δ, as well as JNK and ERK family members [27]. Therefore, PROTACs based on PH-797804 might also be able to induce p38β degradation in cells. We found that both compounds **NR-7h** and **NR-6a** induced the degradation of

p38β in several cancer cell lines (Fig. 6a). However, **NR-7h** and **NR-6a** treatment affected neither the expression levels of p38γ and p38δ nor those of other related MAPK family members such as JNK1/2 and ERK1/2, in any of the cell lines analyzed (Fig. 7a). We estimated that the DC_{50} values of both compounds for p38β were between 19 and 49 nM in two different cancer cell lines (Supporting Information Fig. S4). Interestingly, we extended our observations to non-malignant cell lines, and confirmed that **NR-7h** and **NR-6a** induced the degradation of p38α and p38β in retina epithelial cells, cardiomyocytes and bone marrow derived macrophages (BMDMs) (Fig. 7b). These results indicate that PROTACs **NR-6a** and **NR-7h** are able to target specifically p38α and p38β but not other related MAPK family members in a variety of cell types.

Next, we confirmed that treatment of cells with **NR-7h** or **NR-6a** did not change the p38α and p38β mRNA expression levels (Supporting Information Fig. S5a), suggesting that the reduced expression levels of p38α and p38β induced by these compounds was due to protein degradation. Furthermore, the ability of **NR-7h** and **NR-6a** to induce p38α and p38β downregulation was blocked when cells were pre-treated with the proteasome inhibitor bortezomib or with the NEDD8-Activating Enzyme (NAE) inhibitor, which prevents activation of cullin-RING ubiquitin ligases like CRBN (Supporting Information Fig. S5b). The data indicate that indeed these PROTACs target p38α and p38β proteins for degradation by the proteasome pathway in a CRBN ubiquitin ligase dependent manner.

To address the specificity of the PROTACs, we performed a proteomic study. MDA-MB-231 cells were subjected to a protocol of stable isotope labeling by amino acids in cell culture (SILAC) until they reached 95% or higher labeling, and then were incubated for 16 h with DMSO or **NR-7h**. Whole protein lysates were prepared and digested, and the peptides were analyzed by mass spectrometry (MS). We identified 17423 unique peptides that corresponded to 2812 protein groups, of which p38α was the most downregulated protein in **NR-7h**-treated cells (Fig. 8).

2.3 PROTACs impair p38α pathway activation in cells.

p38α is activated by a broad range of cellular stimuli including many stresses and pro-inflammatory cytokines. We analyzed the ability of the PROTACs to inhibit the p38α pathway activity in cells. Using MDA-MB-231 cancer cells, we detected a robust upregulation of MK2 phosphorylation in response to ultraviolet light (UV), which was strongly reduced upon incubation with PH-797804 or the PROTACs (Fig. 9a). Since UV-

induced phosphorylation of MK2 is known to depend mostly on p38α activity, the results indicate that PROTAC treatment efficiently downregulates this signaling pathway in cells. We also confirmed that the *N*-methyl inactive controls **NR-7h*** and **NR-6a*** did not induce p38α protein degradation, but surprisingly compound **NR-7h*** was able to inhibit p38α signaling, probably because the PH-797804 component of the PROTAC remains active. On the other hand, **NR-6a*** does not inhibit p38α signaling despite possessing the same warhead, differing only in the linker and E3 ligase exit vector. Moreover, the inhibition of p38α was observed for at least two days after addition of the PROTACs to the cell culture media (Fig. 9b). To further validate the effect of PROTACs on p38α signaling beyond cancer cells, we used BMDMs, which are known to activate the p38α pathway in response to lipopolysaccharide (LPS) and interferon (IFN)-γ stimulation. Accordingly, we detected a robust phosphorylation of MK2 in cells treated with LPS and IFN-γ, which was strongly reduced upon incubation with PH-797804 or the PROTACs (Fig. 9c). These results indicate that PROTAC treatment can efficiently downregulate the p38α signaling pathway in primary cells.

3. Discussion

In this manuscript, we report the design, synthesis and characterization of small molecules that can trigger p38α downregulation in mammalian cells. These PROTACs were based on an ATP competitive inhibitor of p38α and p38β (PH-797804) that was linked to thalidomide analogues to recruit CRBN E3 ligases. Our work confirms the importance of the length and composition of the linker to bring together the target protein and the E3 ligase in the correct spatial orientation so that a productive protein-protein interaction is formed that ultimately allows ubiquitination of the target protein [12]. Accordingly, we found that an appropriate linker length is critical for the activity of PROTACs that target p38α, with linkers having 15-17 atoms showing optimal performance, which is longer than most PROTACs for other targets [26, 28]. Moreover, we observed that compounds with the same linker but that differ only in their connection to thalidomide (i.e., **NR-3c** and **NR-4**) showed different abilities to induce p38α degradation, emphasizing the importance of the exit vector of the thalidomide fragment in engaging productive CRBN binding.

Our work allowed us to identify several PROTACs that induce the degradation of both p38α and p38β, without affecting other MAPKs, when administered at nanomolar concentrations to the culture medium of several cell lines. These PROTACs show a distinct

selectivity profile over the recently reported p38α degrader SJFα, which also degrades p38δ at nanomolar concentrations, albeit higher than for p38α, and presumably degrades c-Met kinase too [13, 21]. Moreover, we provide evidence that these PROTACs can function in several cell types, including epithelial cells, cardiomyocytes and macrophages.

Protein degradation is thought to have several benefits over traditional inhibition of the enzymatic activity. For example, it does not depend on occupation of the active site of the target protein, requiring only a transient binding effect in order to initiate degradation, therefore enabling sub-stoichiometric quantities of PROTAC to be used [11]. However, our initial characterization did not show a marked improvement in the extent of p38α pathway inhibition in cells, as determined by the phosphorylation of the p38α substrate MK2, for **NR-6a** or **NR-7h** compared to PH-797804. This might be due to the potent inhibitory capacity of PH-797804 being difficult to improve upon. Further work will be needed to determine if particular p38α functions could be differentially affected by PROTACs and chemical inhibitors, but our observations highlight the need for further understanding the advantages and mechanisms of PROTAC-induced degradation for each given target.

An important consideration for PROTAC use is that the degraded protein's function is subdued until new protein synthesis has taken place. This generally lasts longer than inhibition of the target protein, which requires occupation of the active site and is therefore limited by the off-rate of the inhibitor. Indeed, the rate of degradation and subsequent re-synthesis is vital for selecting an appropriate target for development of novel PROTAC therapies. It should be noted that p38α expression is maintained to minimal levels for several days, suggesting that protein re-synthesis is not a limiting factor for the use of p38α-targeted PROTACs.

Further work will be needed to explore the therapeutic potential of using PROTACs to target p38α for degradation, and whether this approach provides any advantage over the use of traditional inhibitors that target p38α kinase activity. These tool compounds should also allow further investigation of the poorly understood pseudo-kinase activity of p38α and determination of its role in diseases.

4. Experimental section

4.1. Chemical synthesis.

General.

All compounds were chemically synthesized, purified by chromatography and characterized by ^{1}H NMR, ^{13}C NMR, IR and HRMS. Compounds were of a purity ≥95% as determined by HRMS and ^{13}C NMR spectroscopy, or by HPLC/ms. NMR spectra were recorded at 23°C on a Varian Mercury 400 or Varian 500 apparatus. ^{1}H NMR and ^{13}C NMR spectra were referenced either to relative internal TMS or to residual solvent peaks. Signal multiplicities in the ^{13}C NMR spectra were assigned by HSQC or DEPT experiments. Melting points were determined using a Büchi M-540 apparatus or by DSC without recrystallization of the final solids. IR spectra were recorded in a Thermo Nicolet Nexus FT-IR apparatus by depositing a film of the product on a sodium chloride disk. HRMS were recorded in a LTQ-FT Ultra (Thermo Scientific) using Nanoelectrospray technique. HPLC chromatography was performed on Hewlett-Packard 1050 equipment with UV detection using a Kinetix EVO C18 50x 4.6 mm, 2.6 μm column (Standard gradient: 10 mM NH_4CO_3 / MeCN (95:5) – (0:100)). PH-797804 was prepared according to literature precedents [16].

The synthesis of compounds **NR-1-5** and **NR-7i-j** and their intermediates is described in the Supporting Information.

Amide formation (General procedure D).

The carboxylic acid (1 equiv) was dissolved in anhydrous DMF, cooled to 0°C, then added Oxyma (ethyl cyanohydroxyiminoacetate**)** (1.66 equiv) and DIC (*N,N′*-Diisopropylcarbodiimide) (1.66 equiv). After 15 min the solution turned yellow, then NEt_3 (1.66 mL) was added, followed by the corresponding amine starting material (1.1 equiv). The reaction was left 18 – 24 h before quenching with water. The mixture was separated between EtOAc and water, then the aqueous layer re-extracted using EtOAc. The combined organic layers were washed with brine, dried over $MgSO_4$, and then concentrated by rotary evaporator under reduced pressure. The corresponding crude amide was then purified by flash column chromatography.

Click reaction (General procedure E).

To a solution of the azide component (1 equiv) in t-BuOH (1.0 mmol mL^{-1}) and water (1.0 mmol mL^{-1}) at 30°C was added $CuSO_4$ (0.3 equiv), sodium ascorbate (0.1 equiv) and the alkyne component (1 equiv). The reaction mixture was then degassed using N_2 for 20 min, then left to stir at this temperature for 20 h. The reaction mixture was then separated between

EtOAc and water, the aqueous layer re-extracted using EtOAc (x3). The combined organic layers were then washed with water and brine, dried over $MgSO_4$ and concentrated under reduced pressure to afford a fluorescent yellow film. The crude was then purified by flash column chromatography, to afford the desired product.

*3-(5-Bromo-4-((2,4-difluorobenzyl)oxy)-6-methyl-2-oxopyridin-1(2H)-yl)-N-(hex-5-yn-1-yl)-4-methylbenzamide (**8a**)*

Following the *general procedure D* starting from **1** and hex-5-yn-1-aminium chloride (**7a**), compound **8a** was obtained in 77% yield. The product eluted from the silica column at 70% EtOAc/hexanes, as a light beige, foamy solid. **TLC: R_f =** 0.36 (50% EtOAc/hexanes). **Mp:** 142–143 °C. **^{1}H NMR (400 MHz, $CDCl_3$)** δ 7.79 (dd, *J* = 8, 2 Hz, 1H), 7.61 (td, *J* = 9, 6 Hz, 1H), 7.50 (d, *J* = 2 Hz, 1H), 7.36 (dd, *J* = 8, 1 Hz, 1H), 7.01 – 6.92 (m, 1H), 6.84 (ddd, *J* = 10, 9, 3 Hz, 1H), 6.74 (NH, t, *J* = 6 Hz, 1H), 6.14 (d, *J* = 1 Hz, 1H), 5.22 (d, *J* = 1 Hz, 2H), 3.39 – 3.21 (m, 2H), 2.21 (td, *J* = 7, 3 Hz, 2H), 2.08 (s, 3H), 1.94 (t, *J* = 3 Hz, 1H), 1.92 (d, *J* = 2 Hz, 3H), 1.66 – 1.52 (m, 3H) ppm. **^{13}C NMR (101 MHz, $CDCl_3$)** δ 165.9 (C), 164.2 (d, J_F = 12 Hz, C), 163.2 (C), 161.4 (dd, J_F = 57, 12 Hz, C), 160.4 (C), 158.7 (d, J_F = 12 Hz, C), 146.4 (C), 138.4 (C), 137.3 (C), 134.4 (C), 131.4 (CH), 130.0 (dd, J_F = 10, 5 Hz, CH), 128.5 (CH), 126.4 (CH), 118.5 (dd, J_F = 14, 4 Hz, C), 111.9 (dd, J_F = 21, 4 Hz, CH), 103.9 (t, J_F = 25 Hz, CH), 96.3 (CH), 84.2 (C), 68.6 (CH), 64.4 (d, J_F = 4 Hz, CH_2), 39.6 (CH_2), 28.4 (CH_2), 25.8 (CH_2), 21.6 (CH_3), 18.1 (CH_2), 17.3 (CH_3) ppm. **IR (NaCl) υ_{max}:** 3304, 2925, 1640, 1527, 1340, 1101 cm^{-1}. **HRMS (ESI):** calc. for $[C_{27}H_{26}O_3N_2BrF_2]^+$: 543.10894 found 543.10700.

*3-(3-Bromo-4-((2,4-difluorobenzyl)oxy)-6-methyl-2-oxopyridin-1(2H)-yl)-4-methyl-N-(pent-4-yn-1-yl)benzamide (**8b**)*

Following the *general procedure D* starting from **1** and pent-4-yn-1-aminium chloride, compound **7b** was obtained in 73% yield. The product eluted from the silica column at 70% EtOAc/hexanes, as a white solid. **TLC: R_f =** 0.43 (80% EtOAc/hexanes). **Mp:** 144–145 °C. **^{1}H NMR (400 MHz, $CDCl_3$)** δ 7.82 (dd, *J* = 8, 2 Hz, 1H), 7.61 (td, *J* = 9, 6 Hz, 1H), 7.54 (d, *J* = 2 Hz, 1H), 7.37 (dd, *J* = 8, 1 Hz, 1H), 7.00 – 6.93 (m, 1H), 6.91 (NH, t, *J* = 6 Hz, 1H), 6.83 (ddd, *J* = 10, 9, 3 Hz, 1H), 6.14 (d, *J* = 1 Hz, 1H), 5.20 (s, 2H), 3.45 – 3.25 (m, 2H), 2.22 (td, *J* = 7, 3 Hz, 2H), 2.08 (s, 3H), 1.96 (t, *J* = 3 Hz, 1H), 1.92 (d, *J* = 1 Hz, 3H), 1.71 (p, *J* = 7 Hz, 2H) ppm. **^{13}C NMR (101 MHz, $CDCl_3$)** δ 165.8 (C), 164.2 (d, J_F = 12 Hz, C), 163.2 (C), 161.4 (dd, J_F = 60, 12 Hz, C), 160.3 (C), 158.6 (d, J_F = 12 Hz, C), 146.5 (C), 138.4 (C), 137.3 (C), 134.2 (C), 131.4 (CH), 129.8 (dd, J_F = 10, 5 Hz, CH), 128.7 (CH), 126.4 (CH), 118.5 (dd, J_F =

14, 4 Hz, C), 111.9 (dd, J_F = 21, 4 Hz, CH), 103.9 (t, J_F = 25 Hz, CH), 96.4 (CH), 83.9 (C), 68.9 (CH), 64.4 (d, J_F = 4 Hz, CH_2), 39.3 (CH_2), 27.9 (CH_2), 21.6 (CH_3), 17.3 (CH_3), 16.2 (CH_2) ppm. **IR (NaCl) υ_{max}:** 3299, 2929, 1644, 1527, 1340, 1088 cm^{-1}. **HRMS (ESI):** calc. for $[C_{26}H_{24}O_3N_2BrF_2]^+$: 529.09329, found 529.09285.

*3-(3-Bromo-4-((2,4-difluorobenzyl)oxy)-6-methyl-2-oxopyridin-1(2H)-yl)-N-(but-3-yn-1-yl)-4-methylbenzamide (**8c**)*

Following the *general procedure D* starting from **1** and but-3-yn-1-aminium chloride (**7c**), compound **8c** was obtained in 50% yield. The product eluted from the silica column at 70% EtOAc/hexanes, as a white solid. **TLC: R_f =** 0.63 (80% EtOAc/hexanes). **Mp:** 148–149 °C. **^{1}H NMR (400 MHz, $CDCl_3$)** δ 7.73 (dd, *J* = 8, 2 Hz, 1H), 7.54 (td, *J* = 8, 6 Hz, 1H), 7.45 (d, *J* = 2 Hz, 1H), 7.31 (dd, *J* = 8, 1 Hz, 1H), 6.90 (tdd, *J* = 9, 3, 1 Hz, 1H), 6.85 (NH, t, *J* = 6 Hz, 1H), 6.78 (ddd, *J* = 10, 9, 3 Hz, 1H), 6.08 (d, *J* = 1 Hz, 1H), 5.16 (s, 2H), 3.38 (dtd, *J* = 43, 13, 7 Hz, 2H), 2.34 (td, *J* = 7, 3 Hz, 2H), 2.03 (s, 3H), 1.92 (t, *J* = 3 Hz, 1H), 1.85 (s, 3H) ppm. **^{13}C NMR (101 MHz, $CDCl_3$)** δ 165.8 (C), 164.2 (d, J_F = 12 Hz, C), 163.2 (C), 161.5 (dd, J_F = 56, 12 Hz, C), 160.4 (C), 158.7 (d, J_F = 12 Hz, C), 146.3 (C), 138.7 (C), 137.5 (C), 134.1 (C), 131.4 (CH), 130.0 (dd, J_F = 10, 5 Hz, CH), 128.4 (CH), 126.5 (CH), 118.5 (dd, J_F = 14, 4 Hz, C), 111.9 (dd, J_F = 21, 4 Hz, CH), 104.3 – 103.5 (m, CH), 96.3 (CH), 81.6 (C), 69.8 (CH), 64.4 (d, J_F = 4 Hz, CH_2), 38.8 (CH_2), 21.6 (CH_3), 19.2 (CH_2), 17.3 (CH_3) ppm. **IR (NaCl) υ_{max}:** 3304, 2933, 1649, 1527, 1349, 1088 cm^{-1}. **HRMS (ESI):** calc. for $[C_{25}H_{22}O_3N_2BrF_2]^+$: 515.07764, found 515.07740.

*3-(3-Bromo-4-((2,4-difluorobenzyl)oxy)-6-methyl-2-oxopyridin-1(2H)-yl)-N-(4-(1-(4-((6-(2-(2,6-dioxopiperidin-3-yl)-1-oxoisoindolin-4-yl)hexyl)amino)-4-oxobutyl)-1H-1,2,3-triazol-4-yl)butyl)-4-methylbenzamide (**NR-6a**)*

Following the *general procedure E* starting from **8a** and **14c**, compound **NR-6a** was obtained as a white solid in 56% yield. **Mp:** 148 ºC. **^{1}H NMR (400 MHz, $CDCl_3$)** δ 9.06 (d, *J* = 15 Hz, 1H), 7.83 (d, *J* = 8 Hz, 1H), 7.69 (d, *J* = 7 Hz, 1H), 7.65 – 7.54 (m, 2H), 7.45 – 7.31 (m, 5H), 7.02 – 6.92 (m, 1H), 6.90 – 6.82 (m, 1H), 6.60 (s, 1H), 6.17 (s, 1H), 5.27 – 5.16 (m, 3H), 4.46 – 4.23 (m, 4H), 3.37 – 3.22 (m, 2H), 3.22 – 3.04 (m, 2H), 2.89 – 2.75 (m, 2H), 2.72 – 2.64 (m, 2H), 2.60 (t, *J* = 8 Hz, 2H), 2.48 – 2.35 (m, 1H), 2.24 – 2.01 (m, 8H), 1.92 (s, 3H), 1.73 – 1.49 (m, 6H), 1.48 – 1.38 (m, 2H), 1.37 – 1.23 (m, 4H) ppm. **^{13}C NMR (101 MHz, CD_3OD)** δ 171.8 (C), 170.2 (C), 169.8 (C), 166.4 (C), 164.4 (d, J_F = 12 Hz, C)163.5 (C), 161.8 (d, J_F = 14 Hz, C), 160.6 (C), 159.0 (d, J_F = 12 Hz, C), 147.8 (C), 146.7 (C), 140.1 (C), 138.7 (C), 137.7 (C), 137.6 (CH), 134.4 (d, J_F = 5 Hz, C), 132.0 (C), 131.6 (CH), 131.4 (CH), 130.5 –

129.9 (m, CH), 128.7 (CH), 128.6 (CH), 126.7 (d, J_F = 2 Hz, CH), 121.9 – 121.4 (m, CH), 118.7 (dd, J_F = 14, 4 Hz, C), 112.1 (dd, J_F = 21, 4 Hz, CH), 104.3 (t, J_F = 25 Hz, CH), 96.7 (CH), 96.5 (C), 64.6 (d, J_F = 4 Hz, CH_2), 51.9 (CH_2), 49.3 (CH), 46.5 (CH_2), 40.0 (CH_2), 39.5 (CH_2), 32.7 (CH_2), 32.1 (CH_2), 30.6 (CH_2), 29.8 (CH_2), 29.4 (CH_2), 29.0 (CH_2), 28.4 (CH_2), 26.7 (CH_2), 26.6 (CH_2), 26.2 (CH_2), 25.1 (CH_2), 23.5 (CH_2), 21.7 (CH_3), 17.4 (CH_3) ppm. **IR (NaCl) υ_{max}:** 3408, 2931, 1644, 1349, 1101 cm^{-1}. **HRMS (ESI):** calc. for $[C_{50}H_{56}O_7N_8BrF_2]^+$: 997.3418; found: 997.3426.

*3-(3-Bromo-4-((2,4-difluorobenzyl)oxy)-6-methyl-2-oxopyridin-1(2H)-yl)-N-(4-(1-(4-((5-(2-(2,6-dioxopiperidin-3-yl)-1-oxoisoindolin-4-yl)pentyl)amino)-4-oxobutyl)-1H-1,2,3-triazol-4-yl)butyl)-4-methylbenzamide (**NR-6b**)*

Following the *general procedure E* starting from **8a** and **14d**, compound **NR-6b** was obtained as a white solid in 26% yield. **Mp:** 136 ºC. **^{1}H NMR (400 MHz, $CDCl_3$)** δ 8.99 (s, 1H), 7.79 (ddd, *J* = 8, 3, 2 Hz, 1H), 7.69 (dt, *J* = 7, 2 Hz, 1H), 7.60 (td, *J* = 9, 6 Hz, 1H), 7.54 (s, 1H), 7.40 (t, *J* = 8 Hz, 1H), 7.37 – 7.31 (m, 3H), 7.26 – 7.16 (m, 1H), 7.01 – 6.93 (m, 1H), 6.86 (ddd, *J* = 10, 9, 3 Hz, 1H), 6.46 (t, *J* = 6 Hz, 1H), 6.15 (dd, *J* = 2, 1 Hz, 1H), 5.25 – 5.17 (m, 3H), 4.42 (dd, *J* = 16, 5 Hz, 1H), 4.35 – 4.26 (m, 3H), 3.37 – 3.25 (m, 2H), 3.23 – 3.05 (m, 2H), 2.88 – 2.79 (m, 1H), 2.69 (t, *J* = 7 Hz, 2H), 2.65 – 2.55 (m, 2H), 2.49 – 2.36 (m, 1H), 2.25 – 2.01 (m, 8H), 1.91 (s, 3H), 1.81 – 1.52 (m, 6H), 1.53 – 1.38 (m, 2H), 1.37 – 1.26 (m, 2H) ppm. **^{13}C NMR (101 MHz, CD_3OD)** δ 171.8 (C), 170.2 (C), 169.8 (C), 167.7 (C), 166.4 (C), 163.5 (C), 162.0 (C), 160.6 (C), 159.1 (C), 148.7 – 147.7 (m, C), 146.7 (C), 143.1 (C), 140.3 (d, J_F = 2 Hz, C), 138.7 (C), 137.6 (C), 137.4 (CH), 134.4 (m, C), 132.0 (C), 131.6 (CH), 131.4 (CH), 130.4 (m, CH), 128.7 (CH), 126.7 (CH), 121.8 (CH), 118.6 (d, J_F = 4 Hz, C), 118.1 – 117.2 (m, CH), 112.08 (dd, J_F = 21, 4 Hz, CH), 104.6 – 103.3 (m, CH), 96.7 (C), 96.5 (CH), 64.7 (d, J_F = 3 Hz, CH_2), 52.0 (CH_2), 49.3 (CH), 46.5 (CH_2), 40.0 (CH_2), 39.4 (CH_2), 32.7 (CH_2), 31.9 (CH_2), 31.8 (CH_2), 29.8 (CH_2), 29.6 (CH_2), 29.3 (CH_2), 28.4 (CH_2), 26.5 (CH_2), 26.2 (CH_2), 25.1 (CH_2), 23.5 (CH_2), 21.7 (CH_3), 17.4 (CH_3) ppm. **IR (NaCl) υ_{max}:** 3385, 2929, 1642, 1528, 1349, 1101 cm^{-1}. **HRMS (ESI):** calc. for $[C_{49}H_{54}O_7N_8BrF_2]^+$: 983.3261; found 983.3238.

*3-(3-Bromo-4-((2,4-difluorobenzyl)oxy)-6-methyl-2-oxopyridin-1(2H)-yl)-N-(2-(1-(4-((2-((2-(2,6-dioxopiperidin-3-yl)-1,3-dioxoisoindolin-4-yl)amino)ethyl)amino)-4-oxobutyl)-1H-1,2,3-triazol-4-yl)ethyl)-4-methylbenzamide (**NR-7a**)*

Following the *general procedure E* starting from **8c** and **15c**, compound **NR-7a** was obtained as a bright yellow solid in 96% yield. **^{1}H NMR (400 MHz, $CDCl_3$)** δ 9.13 (d, *J* = 23 Hz, 1H),

7.69 (t, *J* = 6 Hz, 1H), 7.57 – 7.49 (m, 1H), 7.45 (s, 1H), 7.38 (ddd, *J* = 9, 7, 1 Hz, 2H), 7.31 (s, 1H), 7.24 (t, *J* = 8 Hz, 2H), 6.98 (dd, *J* = 7, 2 Hz, 1H), 6.94 – 6.84 (m, 2H), 6.80 (ddd, *J* = 10, 9, 3 Hz, 1H), 6.36 (s, 1H), 6.09 (d, *J* = 3 Hz, 1H), 5.16 (s, 2H), 4.87 – 4.80 (m, 1H), 4.21 (s, 2H), 3.61 – 3.44 (m, 2H), 3.32 (s, 4H), 2.83 – 2.61 (m, 5H), 1.98 (d, *J* = 14 Hz, 6H), 1.89 – 1.80 (m, 5H) ppm. **^{13}C NMR (101 MHz, $CDCl_3$)** δ 172.6 (C), 171.9 (C), 171.7 (C), 169.2 (C), 169.1 (C), 167.6 (C), 166.2 (d, J_F = 8 Hz, C), 164.5 – 164.1 (m, C), 163.3 (C), 162.0 (C), 161.7 (C), 160.5 (d, *J* = 2 Hz, C), 158.9 (d, J_F = 12 Hz, C), 146.7 (C), 146.4 (C), 138.8 (C), 137.5 (C), 136.2 (CH), 134.0 (d, J_F = 6.3 Hz, C), 132.4 (C), 131.4 (d, J_F = 5 Hz, CH), 130.3 (dd, J_F = 10, 6 Hz, CH), 128.3 (CH), 126.7 (CH), 118.5 (d, J_F = 3 Hz, CH), 116.8 (CH), 111.9 (dd, J_F = 21, 3 Hz, CH), 111.6 (CH), 110.1 (C) , 104.4 – 103.5 (m, CH), 96.4 (CH), 64.5 (d, J_F = 4 Hz, CH_2), 49.1 (CH_2), 48.9 (CH), 42.2 (CH_2), 39.2 (CH_2), 38.6 (CH_2), 31.9 (CH_2), 31.4 (CH_2), 25.7 (CH_2), 25.5 (CH_2), 22.7 (CH_2), 21.5 (CH_3), 17.3 (CH_3) ppm. **IR (NaCl) υ_{max}:** 3338, 2938, 1702, 1641, 1501, 1340, 1040 cm^{-1}. **HRMS (ESI):** calc. for $[C_{44}H_{43}O_8N_9BrF_2]^+$: 942.23805, found 942.23882.

*3-(3-Bromo-4-((2,4-difluorobenzyl)oxy)-6-methyl-2-oxopyridin-1(2H)-yl)-N-(2-(1-(4-((3-((2-(2,6-dioxopiperidin-3-yl)-1,3-dioxoisoindolin-4-yl)amino)propyl)amino)-4-oxobutyl)-1H-1,2,3-triazol-4-yl)ethyl)-4-methylbenzamide (**NR-7b**)*

Following the *general procedure E* starting from **8c** and **15b**, compound **NR-7b** was obtained as a bright yellow solid in 78% yield. **^{1}H NMR (400 MHz, $CDCl_3$)** δ 8.71 (d, *J* = 28.6 Hz, 1H), 7.69 (d, *J* = 8.1 Hz, 1H), 7.53 (q, *J* = 8.1 Hz, 1H), 7.42 (s, 1H), 7.38 (t, *J* = 7.9 Hz, 1H), 7.34 (s, 1H), 7.26 (dd, *J* = 8.1, 3.8 Hz, 1H), 7.21 (s, 1H), 6.98 (d, *J* = 7.0 Hz, 1H), 6.91 (t, *J* = 8.1 Hz, 1H), 6.85 – 6.77 (m, 3H), 6.32 (s, 1H), 6.09 (s, 1H), 5.17 (s, 2H), 4.85 (dd, *J* = 11.6, 5.5 Hz, 1H), 4.27 (d, *J* = 7.2 Hz, 2H), 3.59 (d, *J* = 13.1 Hz, 2H), 3.21 (d, *J* = 6.2 Hz, 4H), 2.86 (s, 2H), 2.76 (t, *J* = 11.6 Hz, 1H), 2.68 (t, *J* = 10.9 Hz, 2H), 2.00 (d, *J* = 27.0 Hz, 7H), 1.90 – 1.80 (m, 4H), 1.70 (t, *J* = 6.6 Hz, 2H) ppm. **^{13}C NMR (101 MHz, $CDCl_3$)** δ 172.1 (2 x C), 171.4 (C), 169.3 (C), 168.7 (C), 167.6 (C), 166.2 (d, J_F = 6 Hz, C), 164.3 (dd, J_F = 13, 3 Hz, C), 163.3 (C), 162.0 (C), 160.7 (C), 160.5 (C), 157.8 (C), 146.7 (C), 146.3 (C), 138.9 (C), 137.5 (C), 136.1 (CH), 134.0 (C), 132.5 (C), 131.5 (CH), 130.4 (CH), 128.2 (CH), 126.5 (CH), 122.5 – 122.0 (m, CH), 118.5 (m, C), 116.7 (CH), 112.0 (dd, J_F = 21, 3 Hz, CH), 111.4 (CH), 110.0 (C), 104.4 – 103.6 (m, CH), 96.4 (CH), 64.4 (d, J_F = 4 Hz, CH_2), 49.3 (CH_2), 48.9 (CH), 40.2 (CH_2), 39.0 (CH_2), 37.0 (CH_2), 31.9 (CH_2), 31.4 (CH_2), 29.0 (CH_2), 25.8 (CH_2), 25.5 (CH_2), 22.8 (CH_2), 21.5 (CH_3), 17.3 (CH_3) ppm. **IR (NaCl) υ_{max}:** 3303, 2925,

1697, 1641, 1501, 1358, 1192 cm^{-1}. **HRMS (ESI):** calc. for $[C_{45}H_{45}O_8N_9BrF_2]^+$: 956.25370, found 956.25392.

*3-(3-Bromo-4-((2,4-difluorobenzyl)oxy)-6-methyl-2-oxopyridin-1(2H)-yl)-N-(3-(1-(4-((3-((2-(2,6-dioxopiperidin-3-yl)-1,3-dioxoisoindolin-4-yl)amino)propyl)amino)-4-oxobutyl)-1H-1,2,3-triazol-4-yl)propyl)-4-methylbenzamide (**NR-7c**)*

Following the *general procedure E* but starting from **8b** and **15b**, compound **NR-7c** was obtained as a bright yellow solid in 52% yield. **^{1}H NMR (400 MHz, $CDCl_3$)** δ 8.90 (d, *J* = 6 Hz, 1H), 7.74 – 7.69 (m, 1H), 7.63 – 7.59 (m, 2H), 7.46 – 7.38 (m, 3H), 7.32 (dd, *J* = 8, 2 Hz, 1H), 7.18 (q, *J* = 5 Hz, 1H), 7.03 (dd, *J* = 7, 2 Hz, 1H), 7.00 – 6.93 (m, 1H), 6.89 – 6.82 (m, 2H), 6.35 (t, *J* = 6 Hz, 1H), 6.18 (t, *J* = 1 Hz, 1H), 5.22 (s, 2H), 4.94 – 4.87 (m, 1H), 4.31 (h, *J* = 8 Hz, 2H), 3.42 (dt, *J* = 12, 6 Hz, 1H), 3.33 – 3.15 (m, 5H), 2.87 – 2.65 (m, 5H), 2.15 – 1.98 (m, 8H), 1.97 – 1.81 (m, 5H), 1.74 (q, *J* = 6 Hz, 2H) ppm. **^{13}C NMR (101 MHz, $CDCl_3$)** δ 172.3 (2 x C), 171.5 (2 x C), 169.3 (C), 168.8 (2 x C), 167.6 (C), 165.7 (C), 165.6 (C), 163.4 (C), 161.6 (dd, J_F = 47, 12 Hz, C), 160.5 (C), 146.7 (C), 146.6 (C), 138.7 (C), 137.5 (C), 136.1 (CH), 133.9 (d, J_F = 8 Hz, C), 132.5 (C), 131.4 (CH), 130.3 (CH), 128.2 (CH), 126.6 (CH), 122.0 (CH), 118.5 (dd, J_F = 15, 5 Hz, C), 116.7 (CH), 111.9 (d, J_F = 25 Hz, CH), 111.3 (CH), 110.0 (d, J_F = 9 Hz, C), 104.0 (t, J_F = 25 Hz, CH), 96.5 (CH), 64.5 (d, J_F = 4 Hz, CH_2), 49.3 (CH_2), 48.9 (CH), 40.1 (CH_2), 39.6 (CH_2), 36.8 (CH_2), 32.0 (CH_2), 31.4 (CH_2), 29.0 (CH_2), 28.2 (CH_2), 25.9 (CH_2), 23.3 (CH_2), 22.8 (CH_2), 21.6 (CH_3), 17.3 (CH_3) ppm. **IR (NaCl) υ_{max}:** 3308, 3082, 2942, 1693, 1641, 1358, 1192, 726 cm^{-1}. **HRMS (ESI):** calc. for $[C_{46}H_{47}O_8N_9BrF_2]^+$: 970.26935, found 970.26913.

*3-(3-Bromo-4-((2,4-difluorobenzyl)oxy)-6-methyl-2-oxopyridin-1(2H)-yl)-N-(2-(1-(4-((4-((2-(2,6-dioxopiperidin-3-yl)-1,3-dioxoisoindolin-4-yl)amino)butyl)amino)-4-oxobutyl)-1H-1,2,3-triazol-4-yl)ethyl)-4-methylbenzamide (**NR-7d**)*

Following the *general procedure E* starting from **8c** and **15a**, compound **NR-7d** was obtained as a bright yellow solid in 99% yield. **^{1}H NMR (400 MHz, $CDCl_3$)** δ 8.93 (d, *J* = 24 Hz, 1H), 7.76 (d, *J* = 8 Hz, 1H), 7.60 (q, *J* = 8 Hz, 1H), 7.51 (s, 1H), 7.48 – 7.31 (m, 4H), 7.06 – 7.02 (m, 1H), 7.01 – 6.93 (m, 1H), 6.90 – 6.81 (m, 2H), 6.78 (s, 1H), 6.21 (s, 1H), 6.16 (s, 1H), 5.23 (s, 2H), 4.91 (dd, *J* = 12, 6 Hz, 1H), 4.33 (s, 2H), 3.62 (d, *J* = 30 Hz, 2H), 3.22 (d, *J* = 18 Hz, 4H), 2.95 – 2.68 (m, 5H), 2.10 (s, 3H), 2.07 – 2.01 (m, 3H), 1.97 – 1.90 (m, 2H), 1.90 – 1.87 (m, 3H), 1.69 – 1.53 (m, 4H) ppm. **^{13}C NMR (101 MHz, $CDCl_3$)** δ 171.8 (C), 171.4 (2 x C), 169.4 (2 x C), 168.8 (C), 167.6 (C), 166.2 (d, J_F = 16 Hz, C), 164.3 (C), 163.3 (C), 161.5

(dd, J_F = 48, 12 Hz, C), 160.4 (d, J_F = 5 Hz, C), 158.8 (d, J_F = 12 Hz, C), 146.8 (C), 146.4 (C), 138.9 (d, J_F = 2 Hz, C), 137.5 (d, J_F = 2 Hz, C), 136.1 (CH), 134.0 (d, J_F = 9 Hz, C), 132.4 (C), 131.6 – 131.3 (m, CH), 130.4 – 130.0 (m, CH), 128.5 – 128.2 (m, CH), 126.6 (CH), 122.3 (CH), 118.5 (dd, J_F = 14, 4 Hz, C), 116.7 (CH), 112.1 – 111.7 (m, CH), 111.4 (CH), 109.8 (d, J_F = 3 Hz, C), 104.0 (t, J = 25 Hz, CH), 96.7 – 96.3 (m, CH), 64.5 (d, J_F = 4 Hz, CH_2), 49.2 (CH_2), 48.9 (CH), 42.2 (CH_2), 39.1 (CH_2), 38.9 (CH_2), 32.0 (d, J_F = 8 Hz, CH_2), 31.4 (CH_2), 26.8 (CH_2), 26.5 (CH_2), 25.9 (CH_2), 25.5 (CH_2), 22.8 (CH_2), 21.5 (CH_3), 17.3 (CH_3) ppm. **IR (NaCl) υ_{max}:** 3299, 2929, 1702, 1641, 1349, 1349, 1044 cm^{-1}. **HRMS (ESI):** calc. for $[C_{46}H_{47}O_8N_9BrF_2]^+$: 970.26935, found 970.26984.

*3-(3-Bromo-4-((2,4-difluorobenzyl)oxy)-6-methyl-2-oxopyridin-1(2H)-yl)-N-(4-(1-(4-((2-((2-(2,6-dioxopiperidin-3-yl)-1,3-dioxoisoindolin-4-yl)amino)ethyl)amino)-4-oxobutyl)-1H-1,2,3-triazol-4-yl)butyl)-4-methylbenzamide (**NR-7e**)*

Following the *general procedure E* starting from **8a** and **15c**, compound **NR-7e** was obtained as a bright yellow solid in 96% yield. **^{1}H NMR (400 MHz, $CDCl_3$)** δ 9.07 (d, J = 53 Hz, 1H), 7.81 – 7.75 (m, 1H), 7.60 (td, J = 8, 6 Hz, 1H), 7.51 (dd, J = 4, 2 Hz, 1H), 7.45 (dd, J = 9, 7 Hz, 1H), 7.34 (dd, J = 15, 7 Hz, 4H), 7.04 (dd, J = 7, 3 Hz, 1H), 7.00 – 6.90 (m, 2H), 6.86 (ddd, J = 11, 9, 3 Hz, 1H), 6.40 (t, J = 5 Hz, 1H), 6.17 (dd, J = 2, 1 Hz, 1H), 5.22 (s, 2H), 4.92 – 4.84 (m, 1H), 4.36 – 4.26 (m, 2H), 3.52 – 3.41 (m, 1H), 3.41 – 3.29 (m, 3H), 3.16 (ddd, J = 30, 14, 7 Hz, 2H), 2.83 – 2.59 (m, 5H), 2.18 – 2.01 (m, 8H), 1.93 – 1.88 (m, 3H), 1.60 (dt, J = 16, 7 Hz, 2H), 1.48 (t, J = 7 Hz, 2H) ppm. **^{13}C NMR (101 MHz, $CDCl_3$)** δ 172.6 (C), 171.6 (2 x C), 169.2 (d, J_F = 5 Hz, C), 169.0 (C), 167.5 (2 x C), 166.5 (C), 166.2 (C), 163.3 (C), 161.7 (C), 160.5 (d, J_F = 7 Hz, C), 146.7 (C), 146.5 (d, J_F = 3 Hz, C), 138.6 (d, J_F = 5 Hz, C), 137.4 (d, J_F = 2 Hz, C), 136.1 (d, J_F = 2 Hz, CH), 134.2 (d, J_F = 20 Hz, C), 132.4 (C), 131.4 (CH), 130.3 (CH), 128.5 (CH), 126.6 (d, J = 10 Hz, CH), 121.7 (CH), 118.5 (d, J_F = 14 Hz, C), 116.8 (CH), 111.9 (dd, J_F = 22, 4 Hz, CH), 111.6 (CH), 110.0 (d, J_F = 4 Hz, C), 104.0 (t, J_F = 25 Hz, CH), 96.6 (d, J_F = 5 Hz, C), 96.4 (CH), 64.5 (d, J_F = 4 Hz, CH_2), 49.2 (d, J = 8 Hz, CH_2), 48.8 (d, J = 3 Hz, CH), 42.20 (d, J = 10 Hz, CH_2), 39.8 (CH_2), 38.8 (d, J = 6 Hz, CH_2), 32.2 (d, J = 20 Hz, CH_2), 31.4 (CH_2), 28.1 (CH_2), 26.3 (CH_2), 25.7 (d, J = 11 Hz, CH_2), 24.8 (CH_2), 22.7 (CH_2), 21.5 (CH_3), 17.3 (CH_3) ppm. **IR (NaCl) υ_{max}:** 3307, 2929, 1693, 1641, 1353, 1196, 731 cm^{-1}. **HRMS (ESI):** calc. for $[C_{46}H_{47}O_8N_9BrF_2]^+$: 970.26935, found 970.26872.

*3-(3-Bromo-4-((2,4-difluorobenzyl)oxy)-6-methyl-2-oxopyridin-1(2H)-yl)-N-(3-(1-(4-((4-((2-(2,6-dioxopiperidin-3-yl)-1,3-dioxoisoindolin-4-yl)amino)butyl)amino)-4-oxobutyl)-1H-1,2,3-triazol-4-yl)propyl)-4-methylbenzamide (**NR-7f**)*

Following the *general procedure E* starting from **8b** and **15a**, compound **NR-7f** was obtained as a bright yellow solid in 53% yield. **^{1}H NMR (400 MHz, $CDCl_3$)** δ 8.78 (d, *J* = 11 Hz, 1H), 7.71 (d, *J* = 8 Hz, 1H), 7.63 – 7.53 (m, 2H), 7.44 (ddd, *J* = 9, 7, 5 Hz, 1H), 7.40 – 7.31 (m, 2H), 7.07 – 6.93 (m, 2H), 6.90 – 6.82 (m, 2H), 6.17 (s, 2H), 5.22 (s, 2H), 4.90 (dd, *J* = 12, 6 Hz, 1H), 4.33 (dt, *J* = 11, 7 Hz, 2H), 3.42 (dd, *J* = 13, 6 Hz, 1H), 3.34 – 3.17 (m, 4H), 3.09 (td, *J* = 14, 13, 6 Hz, 1H), 2.88 – 2.66 (m, 6H), 2.09 (d, *J* = 7 Hz, 3H), 2.06 (d, *J* = 2 Hz, 3H), 1.99 (q, *J* = 7 Hz, 1H), 1.95 – 1.85 (m, 6H), 1.63 – 1.47 (m, 5H) ppm. **^{13}C NMR (101 MHz, $CDCl_3$)** δ 172.0 (d, *J* = 4 Hz, C), 171.3 (2 x C), 169.4 (C), 168.8 (d, *J* = 4 Hz, C), 167.6 (2 x C), 165.8 (2 x C), 163.4 (d, *J* = 3 Hz, C), 160.5 (d, *J* = 9 Hz, C), 146.8 (C), 146.5 (d, *J* = 5 Hz, C), 138.7 (d, *J* = 6 Hz, C), 137.6 (C), 136.1 (CH), 134.0 (C), 132.4 (C), 131.4 (CH), 130.5 – 130.0 (m, CH), 128.1 (CH), 126.7 (CH), 122.0 (d, *J* = 6 Hz, CH), 118.4 (C), 116.7 (CH), 112.2 – 111.6 (m, CH), 111.3 (d, *J* = 3 Hz, CH), 109.7 (C), 104.46 – 103.41 (m, CH), 96.6 (CH), 96.4 (C), 64.5 (d, J_F = 4 Hz, CH_2), 49.3 (d, *J* = 9 Hz, CH_2), 48.9 (d, *J* = 2 Hz CH), 42.1 (CH_2), 39.7 (CH_2), 39.5 (CH_2), 38.8 (CH_2), 31.9 (d, *J* = 10 Hz, CH_2), 31.4 (CH_2), 28.3 (CH_2), 26.7 (d, *J* = 30 Hz, CH_2), 25.9 (CH_2), 23.2 (CH_2), 22.8 (CH_2), 21.5 (CH_3), 17.3 (CH_3) ppm. (1 C not observed in spectrum) **IR (NaCl) υ_{max}:** 3308, 3090, 2920, 1697, 1640, 1353, 726 cm^{-1}. **HRMS (ESI):** calc. for $[C_{47}H_{49}O_8N_9BrF_2]^+$: 984.28500, found 984.28549.

*3-(3-Bromo-4-((2,4-difluorobenzyl)oxy)-6-methyl-2-oxopyridin-1(2H)-yl)-N-(4-(1-(4-((3-((2-(2,6-dioxopiperidin-3-yl)-1,3-dioxoisoindolin-4-yl)amino)propyl)amino)-4-oxobutyl)-1H-1,2,3-triazol-4-yl)butyl)-4-methylbenzamide (**NR-7g**)*

Following the *general procedure E* starting from **8a** and **15b**, compound **NR-7g** was obtained as a bright yellow waxy solid in 44% yield. **^{1}H NMR (400 MHz, $CDCl_3$)** δ 8.93 (d, *J* = 11 Hz, 1H), 7.71 (d, *J* = 8 Hz, 1H), 7.53 (td, *J* = 9, 6 Hz, 1H), 7.48 (s, 1H), 7.37 (t, *J* = 8 Hz, 1H), 7.26 (d, *J* = 8 Hz, 1H), 7.00 – 6.86 (m, 3H), 6.82 – 6.75 (m, 2H), 6.30 (s, 1H), 6.10 (s, 1H), 5.15 (s, 2H), 4.89 – 4.81 (m, 1H), 4.26 (s, 2H), 3.20 (s, 7H), 2.78 – 2.51 (m, 5H), 2.06 (d, *J* = 30 Hz, 6H), 1.97 (d, *J* = 1 Hz, 3H), 1.83 (s, 3H), 1.69 (t, *J* = 6 Hz, 2H), 1.58 (s, 2H), 1.44 (s, 2H) ppm. **^{13}C NMR (101 MHz, $CDCl_3$)** δ 172.2 (C), 171.6 (d, *J* = 4 Hz, C), 169.3 (C), 168.9 (d, *J* = 4 Hz, C), 167.6 (C), 166.2 (d, *J* = 8 Hz, C), 164.2 (C), 163.3 (C), 161.8 (d, *J* = 12 Hz, C), 161.3 (d, *J* = 12 Hz, C), 160.5 (C), 158.8 (d, *J* = 12 Hz, C), 146.6 (d, *J* = 7 Hz, C), 138.5 (C), 137.4 (C), 136.1 (CH), 134.2 (d, *J* = 7 Hz, C), 132.5 (C), 131.4 (CH), 130.2 (dd, *J* = 10, 5

Hz, CH), 128.5 (CH), 126.5 (CH), 118.5 (dd, *J* = 14, 4 Hz, C), 116.7 (CH), 111.9 (dd, *J* = 21, 4 Hz, CH), 111.3 (CH), 109.9 (C), 103.9 (t, *J* = 25 Hz, CH), 96.5 (d, *J* = 9 Hz, CH), 64.5 (d, *J* = 4 Hz, CH_2), 49.3 (CH_2), 48.9 (CH), 40.1 (CH_2), 39.8 (CH_2), 36.9 (CH_2), 32.4 (CH_2), 31.4 (CH_2), 29.0 (CH_2), 28.2 (CH_2), 26.3 (CH_2), 25.8 (CH_2), 24.9 (CH_2), 22.8 (CH_2), 21.6 (CH_3), 17.3 (CH_3) ppm. **IR (NaCl) υ_{max}:** 3282, 2929, 1702, 1644, 1349, 1192, 1031 cm^{-1}. **HRMS (ESI):** calc. for $[C_{47}H_{49}O_8N_9BrF_2]^+$: 984.28531, found 984.28505.

*3-(3-Bromo-4-((2,4-difluorobenzyl)oxy)-6-methyl-2-oxopyridin-1(2H)-yl)-N-(4-(1-(4-((4-((2-(2,6-dioxopiperidin-3-yl)-1,3-dioxoisoindolin-4-yl)amino)butyl)amino)-4-oxobutyl)-1H-1,2,3-triazol-4-yl)butyl)-4-methylbenzamide (**NR-7h**)*

Following the *general procedure E* starting from **8a** and **15a**, compound **NR-7h** was obtained as a bright yellow solid in 78% yield. **DSC** = 231.6 °C (peak), 188.7 °C (onset). **^{1}H NMR (400 MHz, $CDCl_3$)** δ 8.84 (d, *J* = 15 Hz, 1H), 7.78 (d, *J* = 8 Hz, 1H), 7.60 (td, *J* = 9, 6 Hz, 1H), 7.53 (bs, 1H), 7.45 (dd, *J* = 9, 7 Hz, 1H), 7.34 (d, *J* = 8 Hz, 2H), 7.21 (s, 1H), 7.04 (dd, *J* = 7, 1 Hz, 1H), 7.00 – 6.92 (m, 1H), 6.88 – 6.72 (m, 3H), 6.20 (dd, *J* = 9, 5 Hz, 1H), 6.16 (s, 1H), 5.22 (s, 2H), 4.95 – 4.85 (m, 1H), 4.32 (t, *J* = 5, 2H), 3.34 – 3.08 (m, 6H), 2.91 – 2.59 (m, 5H), 2.19 – 2.02 (m, 8H), 1.90 (s, 3H), 1.73 – 1.47 (m, 8H) ppm. **^{13}C NMR (101 MHz, $CDCl_3$)** δ 172.0 (C), 171.8 (C), 171.7 (C), 169.6 (C), 169.1 (C), 167.7 (2 x C), 166.1 (d, J_F = 7 Hz, C), 164.4 (C), 163.5 (C), 161.9 (C), 161.8 (C), 160.6 (d, J_F = 3 Hz, C), 146.9 (C), 146.8 (C), 138.6 (d, J_F = 2 Hz, C), 137.5 (C), 136.3 (CH), 134.3 (d, *J* = 4 Hz, C), 132.5 (C), 131.5 (CH), 130.3 (dd, *J* = 10, 4 Hz, CH), 128.7 (CH), 126.7 (CH), 121.9 – 121.2 (m, CH), 118.9 – 118.3 (m, C), 116.9 (CH), 112.0 (dd, J_F = 22, 4 Hz, CH), 111.4 (CH), 109.9 (d, J_F = 3 Hz, C), 104.1 (t, *J* = 25 Hz, CH), 96.6 (CH), 64.7 (d, J_F = 4 Hz, CH_2), 49.4 (CH_2), 49.0 (CH), 42.3 (CH_2), 39.9 (CH_2), 39.0 (CH_2), 32.6 (CH_2), 32.5 (CH_2), 31.6 (CH_2), 27.0 (CH_2), 26.7 (CH_2), 26.6 (CH_2), 26.1 (CH_2), 25.1 (CH_2), 22.9 (CH_2), 21.7 (CH_3), 17.4 (CH_3) ppm. **IR (NaCl) υ_{max}:** 3388, 2925, 1697, 1641, 1354, 1198, 1101 cm^{-1}. **HRMS (ESI):** calc. for $[C_{48}H_{51}O_8N_9BrF_2]^+$: 998.3007, found 998.2978.

4.2. Cell culture and treatments.

Experiments were done using the cancer cell lines BBL358, MB-MDA-231, T47D, and MCF7, HT29, and HeLa, as well as RPE cells, H9c2 cells and BMDMs. MB-MDA-231, T47D, MCF7, HeLa, HT29, RPE and H9c2 cells were purchased from ATCC. BBL358 were generated as described [10] and BMDMs were obtained from bone marrow precursor cells isolated from femurs and tibias of mice. Once isolated BMDMs were incubated in

conditioned media from the mouse fibroblast cell line L929 (L-cell) for 6 days, and then were cultured in complete DMEM as described [8]. All cells were cultured in DMEM or DMEM-F12 according to ATCC recommendations, supplemented with 10% FBS, 1 % L-Glutamine and 1% penicillin-streptomycin at 37ºC and 5% CO_2. For passaging, cells were washed in PBS and incubated in 1 ml trypsin at 37ºC until detached. Then, complete media was added, and cells were diluted as desired depending on the confluence and re-plated in a new culture dish.

Cells were treated with the indicated concentrations of PROTACs or with 2 μM of PH797804 (Selleckchem #S2726). p38α pathway activation was induced with UV (30 J/m^2) or 100 ng/ml LPS (Sigma #L4005) and 50 ng/ml IFNγ (Peprotech #315-05). The proteasome was inhibited with 100 nM bortezomib (Selleckchem #PS-341). The NEDD8-Activating Enzyme (NAE) inhibitor MLN4924 (Calbiochem #505477) was used at 1 μM.

*4.3. Protein extraction and immunoblotting***.**

Cells were lysed in RIPA buffer containing 1% NP40, 0.5% sodium deoxycholate, 0.1% SDS, 50mM Tris-HCl, 150 mM NaCl, 5 mM EDTA, 5 mM EGTA, 20 mM sodium fluoride, 1 mM PMSF, 1 mM sodium orthovanadate, 2.5 mM benzamidine, 10 μg/ml pepstatin A, 1 μM mycrocystin, 10 μg/ml leupeptin and 10 μg/ml aprotinin. Cell lysates were maintained for 15 min on ice and then centrifuged at 13000xg at 4°C for 15 min. Supernatants were collected, separated by SDS polyacrylamide gel electrophoresis and analyzed by immunoblotting. The following antibodies were used: p38α (Santa cruz #sc-81621; 1:500), human p38β (Cell signaling #2339; 1:500), mouse p38β (Thermo Fisher 33-8700, 1:500), p38δ (Cell signaling #2308; 1:1000), p38γ (Cell signaling #2307; 1:1000), phospho-p38 (Cell signaling #9211, 1:1000); Erk1/2 (Cell signaling #9102; 1:1000), phospho-MK2 (Cell signaling #3007; 1:500), α-tubulin (Sigma #T9026; 1:10000), and Jnk (Santa cruz #sc-571; 1:2000). Band intensities were determined using the Odyssey Infrared Imaging System (Li-Cor, Biosciences) and quantified by ImageJ.

4.4. SILAC experiment.

MDA-MB-231 cells were cultured with SILAC medium DMEM F-12 (Invitrogen, USA) without arginine or lysine, and supplemented with 2% dialyzed fetal bovine serum (dFBS) (Invitrogen), 2 g/l glucose (Invitrogen), 0.29 g/l L-glutamine (Invitrogen), 5 mg/l Phenol Red (Invitrogen) and 200 mg/l L-proline (Sigma, USA). “Light” growth medium was additionally

supplemented with 100 mg/l L-lysine (SIGMA), 100 mg/l L-arginine (SIGMA), whereas "heavy" growth medium was supplemented with 100 mg/l heavy lysine ([13C6, 15N2]-L-lysine (SILANTES, Germany)) and 100 mg/l heavy arginine ([13C6, 15N4]-L-arginine (SILANTES, Germany)). Cells labelled with "light" and "heavy" amino acids were treated with DMSO or **NR-7h** (1 μM), respectively, for 16 h, and then were lysed in 0.1 M Tris-HCl, pH 7.6, 4% SDS, 0.1 M DTT at RT and briefly sonicated. Samples were digested in FASP with trypsin overnight at 37ºC following FASP protocol [29]. Digested peptides were diluted in 3% ACN/1% FA. Sample was loaded to a 300 μm × 5 mm PepMap100, 5 μm, 100 Å, C18 μ-precolumn (Thermo Scientific) at a flow rate of 15 μl/min using a Thermo Scientific Dionex Ultimate 3000 chromatographic system (Thermo Scientific). Peptides were separated using a C18 analytical column (nanoEase M/Z HSS C18 T3 100Å, 1.8 μm, 75 μm x 250 mm, Waters) with a 300 min run with a linear gradient from 3 to 35% B in 267 min (A= 0.1% FA in water, B= 0.1% FA in CH3CN). Survey MS scans were acquired in the Orbitrap with the resolution (defined at 200 m/z) set to 120,000. The lock mass was user-defined at 445.12 m/z in each Orbitrap scan. The top speed (most intense) ions per scan were fragmented by CID and detected in the Iontrap. An additional event for targeted mass difference was included (only one of the precursor triplet is fragmented). The ion count target value was 400,000 and 4000 for the survey scan and for the MS/MS scan respectively. Target ions already selected for MS/MS were dynamically excluded for 15s. Spray voltage in the NanoMate source was set to 1.60 kV. RF Lens were tuned to 30%. Minimal signal required to trigger MS to MS/MS switch was set to 5,000.

MS/MS spectra were searched against the SwissProt (human, release 2019_05) and contaminants database using MaxQuant v1.6.6.0 with andromeda search engine [30]. Peptide and fragment mass tolerances were 20 ppm and 0.5 Da respectively. Peptides and proteins were filtered at a false discovery rate (FDR) of 1 % based on the number of hits against the reversed sequence database.

Protein intensities were used for the statistical analysis. Within each SILAC experiment, protein quantitation was normalized to the total intensity for channel and experiment. Data was first transformed to log scale to apply a linear model. For each treatment, 6 samples were analyzed corresponding to three biological replicates with two technical replicates of each biological sample. We filtered the data to retain only proteins with valid quantification values in at least 4 out of 6 samples in at least one group. Missing values were imputed with normally distributed random numbers (centered at -1.8 standard deviations

units and spread 0.3 standard deviations units with respect to non-missing values). To adjust for batch effect a linear model was used with SILAC batch as fixed effect. Model fitting was accomplished with the lmFit function of the limma package [31] of R statistical software (http://www.Rproject.org). Comparison between the two groups (H and L) was done and p-values were adjusted using the Benjamini & Hochberg correction. Proteins with an adjusted p-value lower than 0.05 and fold change higher than 2 were considered statistically significant between groups. Clustering analysis was performed using the Perseus software vs 1.6.3 [32]. The adjusted intensities after removing batch effect were filtered with those proteins significant in at least one comparison and z-score normalized. Clustering was done by using multiple iterations of hierarchical clustering.

4.5. RNA extraction and gene expression analysis.

Total RNA was extracted using PureLink RNA mini kit (Invitrogen) following the manufacturer's instructions. Reverse transcription reactions were performed using 500 ng of total RNA using Superscript IV reverse transcriptase (Invitrogen) following manufacturer's instructions for cDNA synthesis. qRT-PCR reactions were performed in triplicates using 5 ng of cDNA and SYBR Green reagent (Life Technologies #4472954) in a Quant-Studio 6 Flex Instrument (Life Technologies). The following primers were used: ACTCAGATGCCGAAGATGGAAC and GTGCTCAGGACTCCATCTCT for p38α, CCCGGACATATATCCAGTCC and TCACTGCTCAATCTCCAGG for p38β, GGATTTGGTCGTATTGGG and GGAAGATGGTGATGGGATT for GAPDH. GAPDH mRNA levels were used for normalization.

Declaration of competing interest

The authors declare no conflicts of interest.

Author Contributions

C. D. designed and synthesized chemical compounds, analyzed data and wrote the manuscript. C.S.-Z. and X.V. contributed to the design and synthesis of chemical compounds. M.C.-R. and N.G.-P. designed and performed experiments in cells to characterize the activity of the compounds, analyzed data and wrote the manuscript. A.R. and A.R.N. conceived the project, provided funding, supervised the overall study, designed experiments, analyzed data, and wrote the manuscript.

Acknowledgements

We are grateful to Marina Gay, Gianluca Arauz, and the rest of the Mass Spectrrometry facility for help in the design of the SILAC experiment and for analysing the samples, and Oskar Fernandez-Capetillo (CNIO) for inspiring discussions. This work was supported by grants from the Spanish MICINN (SAF2016-81043-R and CTQ2017-87840-P), AGAUR (2017 SRG-557), and "La Caixa" Foundation (Young BioMedTec). C.D. thanks "La Caixa" Foundation for a predoctoral fellowship. IRB Barcelona is the recipient of institutional funding from MINECO through the Centres of Excellence Severo Ochoa award and from the CERCA Program of the Catalan Government.

Appendix A. Supplementary data

Experimental procedures for the synthesis of PROTACs **NR-1-5**, **NR-7i-j**, **NR-7h*** and **NR-6a***, and for the synthesis of all intermediates. Additional figures illustrating the structures and activities of different PROTACs.

Abbreviations used

BMDM, bone-marrow-derived macrophages; DC_{50}, 50% of protein degradation; DIC, *N*,*N*′-diisopropylcarbodiimide, DMEM, dulbecco's modified eagle medium; DMF, dimethylformamide, FBS, fetal bovine serum; LPS, lipopolysaccharide; MAPK, mitogen-activated protein kinase; MS, mass spectrometry; Oxyma, ethyl cyanohydroxyiminoacetate, PROTAC, proteolysis targeted chimera; SDS, sodium dodecyl sulfate; UV, ultraviolet light., NEt_3,

References

[1] A. Cuadrado, A.R. Nebreda, Mechanisms and functions of p38 MAPK signalling, Biochem J, 429 (2010) 403-417.
[2] I. del Barco Barrantes, J.M. Coya, F. Maina, J.S. Arthur, A.R. Nebreda, Genetic analysis of specific and redundant roles for p38alpha and p38beta MAPKs during mouse development, Proc Natl Acad Sci U S A, 108 (2011) 12764-12769.
[3] N. Trempolec, N. Dave-Coll, A.R. Nebreda, SnapShot: p38 MAPK substrates, Cell, 152 (2013) 924-924 e921.
[4] S.C. Karcher, S.A. Laufer, Successful structure-based design of recent p38 MAP kinase inhibitors, Curr Top Med Chem, 9 (2009) 655-676.
[5] T.T. Chou, J.Q. Trojanowski, V.M. Lee, p38 mitogen-activated protein kinase-independent induction of gadd45 expression in nerve growth factor-induced apoptosis in medulloblastomas, The Journal of biological chemistry, 276 (2001) 41120-41127.

[6] L. Fan, X. Yang, J. Du, M. Marshall, K. Blanchard, X. Ye, A novel role of p38 alpha MAPK in mitotic progression independent of its kinase activity, Cell Cycle, 4 (2005) 1616-1624.
[7] A. Igea, A.R. Nebreda, The Stress Kinase p38alpha as a Target for Cancer Therapy, Cancer Res, 75 (2015) 3997-4002.
[8] C. Youssif, M. Cubillos-Rojas, M. Comalada, E. Llonch, C. Perna, N. Djouder, A.R. Nebreda, Myeloid p38alpha signaling promotes intestinal IGF-1 production and inflammation-associated tumorigenesis, EMBO Mol Med, 10 (2018).
[9] M. Curtis, H.A. Kenny, B. Ashcroft, A. Mukherjee, A. Johnson, Y. Zhang, Y. Helou, R. Batlle, X. Liu, N. Gutierrez, X. Gao, S.D. Yamada, R. Lastra, A. Montag, N. Ahsan, J.W. Locasale, A.R. Salomon, A.R. Nebreda, E. Lengyel, Fibroblasts Mobilize Tumor Cell Glycogen to Promote Proliferation and Metastasis, Cell Metab, 29 (2019) 141-155 e149.
[10] B. Canovas, A. Igea, A.A. Sartori, R.R. Gomis, T.T. Paull, M. Isoda, H. Perez-Montoyo, V. Serra, E. Gonzalez-Suarez, T.H. Stracker, A.R. Nebreda, Targeting p38alpha Increases DNA Damage, Chromosome Instability, and the Anti-tumoral Response to Taxanes in Breast Cancer Cells, Cancer Cell, 33 (2018) 1094-1110 e1098.
[11] A.C. Lai, C.M. Crews, Induced protein degradation: an emerging drug discovery paradigm, Nat Rev Drug Discov, 16 (2017) 101-114.
[12] K. Cyrus, M. Wehenkel, E.Y. Choi, H.J. Han, H. Lee, H. Swanson, K.B. Kim, Impact of linker length on the activity of PROTACs, Mol Biosyst, 7 (2011) 359-364.
[13] D.P. Bondeson, B.E. Smith, G.M. Burslem, A.D. Buhimschi, J. Hines, S. Jaime-Figueroa, J. Wang, B.D. Hamman, A. Ishchenko, C.M. Crews, Lessons in PROTAC Design from Selective Degradation with a Promiscuous Warhead, Cell Chem Biol, 25 (2018) 78-87 e75.
[14] M. Xi, Y. Chen, H. Yang, H. Xu, K. Du, C. Wu, Y. Xu, L. Deng, X. Luo, L. Yu, Y. Wu, X. Gao, T. Cai, B. Chen, R. Shen, H. Sun, Small molecule PROTACs in targeted therapy: An emerging strategy to induce protein degradation, Eur J Med Chem, 174 (2019) 159-180.
[15] M. Pettersson, C.M. Crews, PROteolysis TArgeting Chimeras (PROTACs) - Past, present and future, Drug Discov Today Technol, 31 (2019) 15-27.
[16] S.R. Selness, R.V. Devraj, B. Devadas, J.K. Walker, T.L. Boehm, R.C. Durley, H. Shieh, L. Xing, P.V. Rucker, K.D. Jerome, A.G. Benson, L.D. Marrufo, H.M. Madsen, J. Hitchcock, T.J. Owen, L. Christie, M.A. Promo, B.S. Hickory, E. Alvira, W. Naing, R. Blevis-Bal, D. Messing, J. Yang, M.K. Mao, G. Yalamanchili, R. Vonder Embse, J. Hirsch, M. Saabye, S. Bonar, E. Webb, G. Anderson, J.B. Monahan, Discovery of PH-797804, a highly selective and potent inhibitor of p38 MAP kinase, Bioorg Med Chem Lett, 21 (2011) 4066-4071.
[17] D.M. Goldstein, A. Kuglstatter, Y. Lou, M.J. Soth, Selective p38alpha inhibitors clinically evaluated for the treatment of chronic inflammatory disorders, J Med Chem, 53 (2010) 2345-2353.
[18] J. Gupta, I. del Barco Barrantes, A. Igea, S. Sakellariou, I.S. Pateras, V.G. Gorgoulis, A.R. Nebreda, Dual function of p38alpha MAPK in colon cancer: suppression of colitis-associated tumor initiation but requirement for cancer cell survival, Cancer Cell, 25 (2014) 484-500.
[19] L. Xing, H.S. Shieh, S.R. Selness, R.V. Devraj, J.K. Walker, B. Devadas, H.R. Hope, R.P. Compton, J.F. Schindler, J.L. Hirsch, A.G. Benson, R.G. Kurumbail, R.A. Stegeman, J.M. Williams, R.M. Broadus, Z. Walden, J.B. Monahan, Structural bioinformatics-based prediction of exceptional selectivity of p38 MAP kinase inhibitor PH-797804, Biochemistry, 48 (2009) 6402-6411.
[20] T. Ito, H. Ando, T. Suzuki, T. Ogura, K. Hotta, Y. Imamura, Y. Yamaguchi, H. Handa, Identification of a primary target of thalidomide teratogenicity, Science, 327 (2010) 1345-1350.

[21] B.E. Smith, S.L. Wang, S. Jaime-Figueroa, A. Harbin, J. Wang, B.D. Hamman, C.M. Crews, Differential PROTAC substrate specificity dictated by orientation of recruited E3 ligase, Nat Commun, 10 (2019) 131.
[22] H.C. Kolb, M.G. Finn, K.B. Sharpless, Click Chemistry: Diverse Chemical Function from a Few Good Reactions, Angew Chem Int Ed Engl, 40 (2001) 2004-2021.
[23] R.P. Wurz, K. Dellamaggiore, H. Dou, N. Javier, M.C. Lo, J.D. McCarter, D. Mohl, C. Sastri, J.R. Lipford, V.J. Cee, A "Click Chemistry Platform" for the Rapid Synthesis of Bispecific Molecules for Inducing Protein Degradation, J Med Chem, 61 (2018) 453-461.
[24] M.S. Gadd, A. Testa, X. Lucas, K.H. Chan, W. Chen, D.J. Lamont, M. Zengerle, A. Ciulli, Structural basis of PROTAC cooperative recognition for selective protein degradation, Nat Chem Biol, 13 (2017) 514-521.
[25] E.S. Fischer, K. Bohm, J.R. Lydeard, H. Yang, M.B. Stadler, S. Cavadini, J. Nagel, F. Serluca, V. Acker, G.M. Lingaraju, R.B. Tichkule, M. Schebesta, W.C. Forrester, M. Schirle, U. Hassiepen, J. Ottl, M. Hild, R.E. Beckwith, J.W. Harper, J.L. Jenkins, N.H. Thoma, Structure of the DDB1-CRBN E3 ubiquitin ligase in complex with thalidomide, Nature, 512 (2014) 49-53.
[26] B. Zhou, J. Hu, F. Xu, Z. Chen, L. Bai, E. Fernandez-Salas, M. Lin, L. Liu, C.Y. Yang, Y. Zhao, D. McEachern, S. Przybranowski, B. Wen, D. Sun, S. Wang, Discovery of a Small-Molecule Degrader of Bromodomain and Extra-Terminal (BET) Proteins with Picomolar Cellular Potencies and Capable of Achieving Tumor Regression, J Med Chem, 61 (2018) 462-481.
[27] H.R. Hope, G.D. Anderson, B.L. Burnette, R.P. Compton, R.V. Devraj, J.L. Hirsch, R.H. Keith, X. Li, G. Mbalaviele, D.M. Messing, M.J. Saabye, J.F. Schindler, S.R. Selness, L.I. Stillwell, E.G. Webb, J. Zhang, J.B. Monahan, Anti-inflammatory properties of a novel N-phenyl pyridinone inhibitor of p38 mitogen-activated protein kinase: preclinical-to-clinical translation, J Pharmacol Exp Ther, 331 (2009) 882-895.
[28] G.E. Winter, D.L. Buckley, J. Paulk, J.M. Roberts, A. Souza, S. Dhe-Paganon, J.E. Bradner, DRUG DEVELOPMENT. Phthalimide conjugation as a strategy for in vivo target protein degradation, Science, 348 (2015) 1376-1381.
[29] J.R. Wisniewski, A. Zougman, N. Nagaraj, M. Mann, Universal sample preparation method for proteome analysis, Nat Methods, 6 (2009) 359-362.
[30] J. Cox, M. Mann, MaxQuant enables high peptide identification rates, individualized p.p.b.-range mass accuracies and proteome-wide protein quantification, Nat Biotechnol, 26 (2008) 1367-1372.
[31] M.E. Ritchie, B. Phipson, D. Wu, Y. Hu, C.W. Law, W. Shi, G.K. Smyth, limma powers differential expression analyses for RNA-sequencing and microarray studies, Nucleic Acids Res, 43 (2015) e47.
[32] S. Tyanova, T. Temu, P. Sinitcyn, A. Carlson, M.Y. Hein, T. Geiger, M. Mann, J. Cox, The Perseus computational platform for comprehensive analysis of (prote)omics data, Nat Methods, 13 (2016) 731-740.

Figure Legends

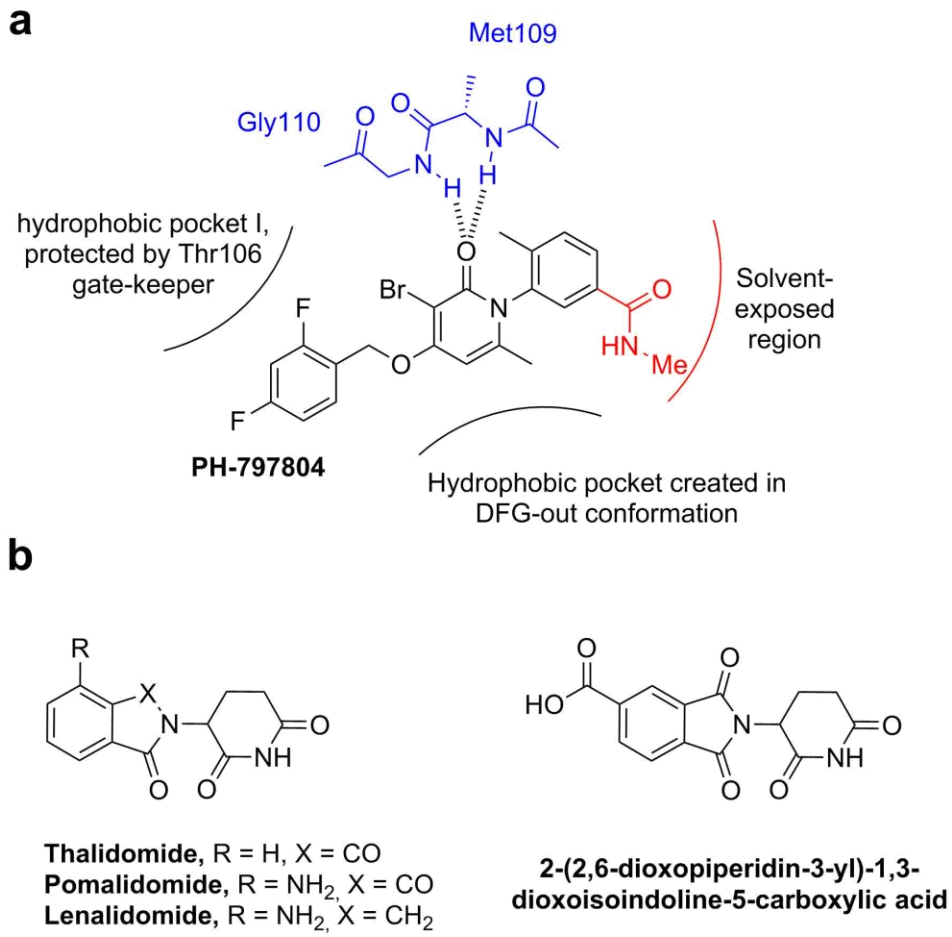

Fig. 1. Molecules used to generate the PROTACs. (a) Diagrammatic representation of the key interactions of PH-797804 within the ATP binding site of p38α, as reported by Xing *et al.* [19]. (b) Formulas of thalidomide, marketed drugs Pomalidomide and Lenalidomide, and a carboxylic acid analogue.

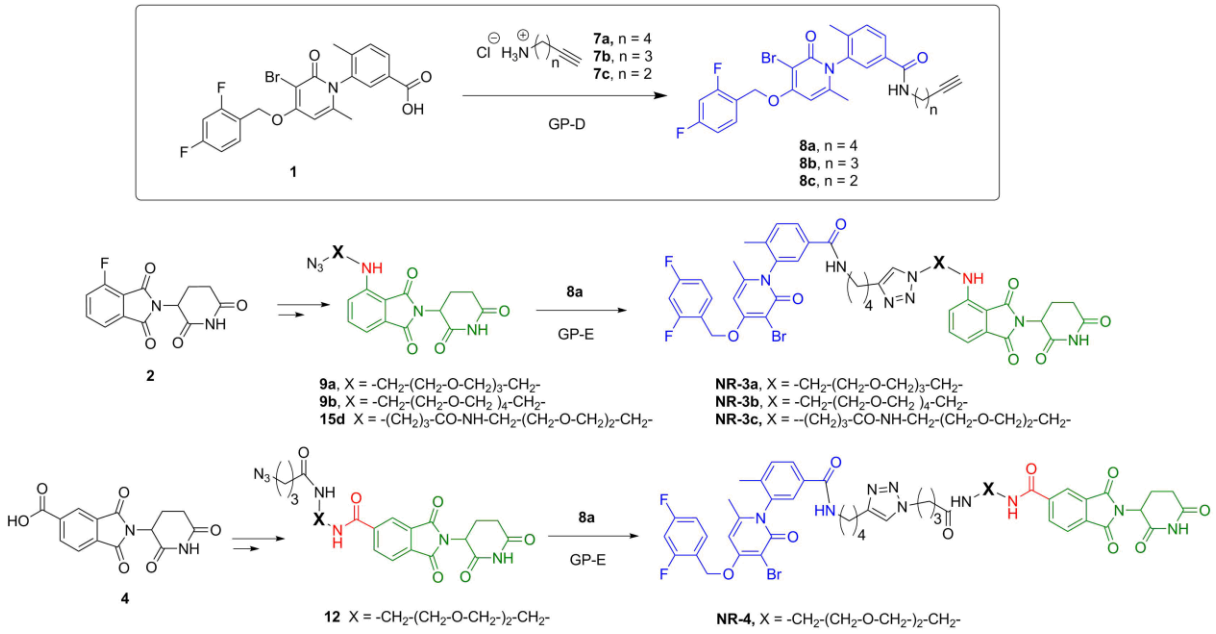

Fig. 2. Synthesis of PROTACs of the general structure **NR-3** and **NR-4**. Reaction conditions. General procedure B (**GP-D**): R-NH_2, Oxyma (ethyl cyanohydroxyiminoacetate), DIC (*N*,*N*′-Diisopropylcarbodiimide), NEt_3, DMF. General procedure E (**GP-E**): CuSO4, Sodium ascorbate, t-BuOH/H_2O 35 ºC.

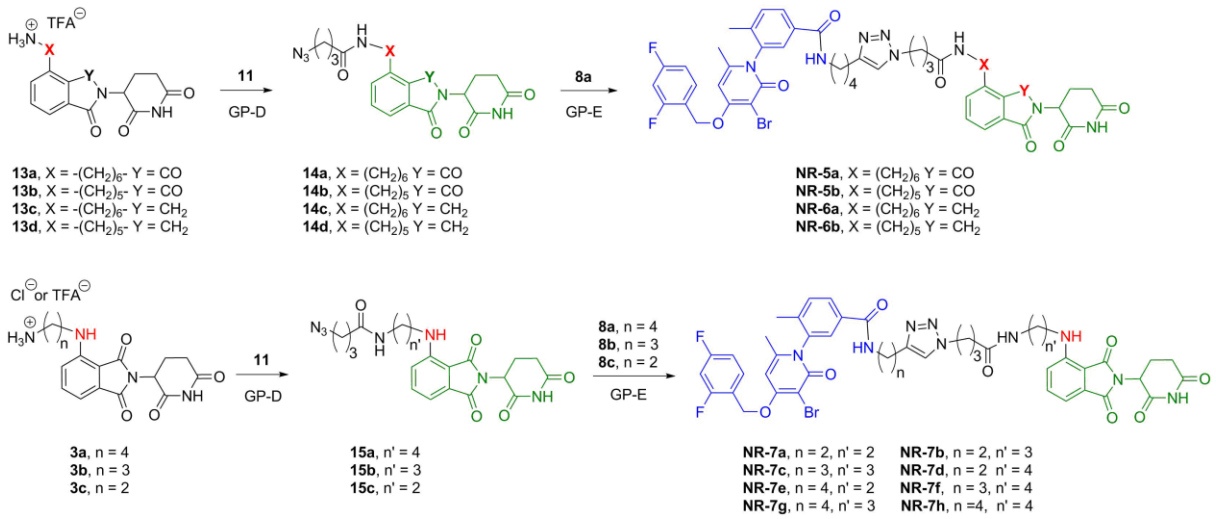

Fig. 3. Synthesis of PROTACs of the general structure **NR-5, NR-6** and **NR-7**. Reaction conditions. General procedure C (**GP-D**): 4-azidobutanoic acid (**11**), Oxyma (ethyl cyanohydroxyiminoacetate), DIC (*N*,*N*′-Diisopropylcarbodiimide), NEt_3, DMF. General procedure E (**GP-E**): CuSO4, Sodium ascorbate, t-BuOH/H_2O 35 ºC.

a)

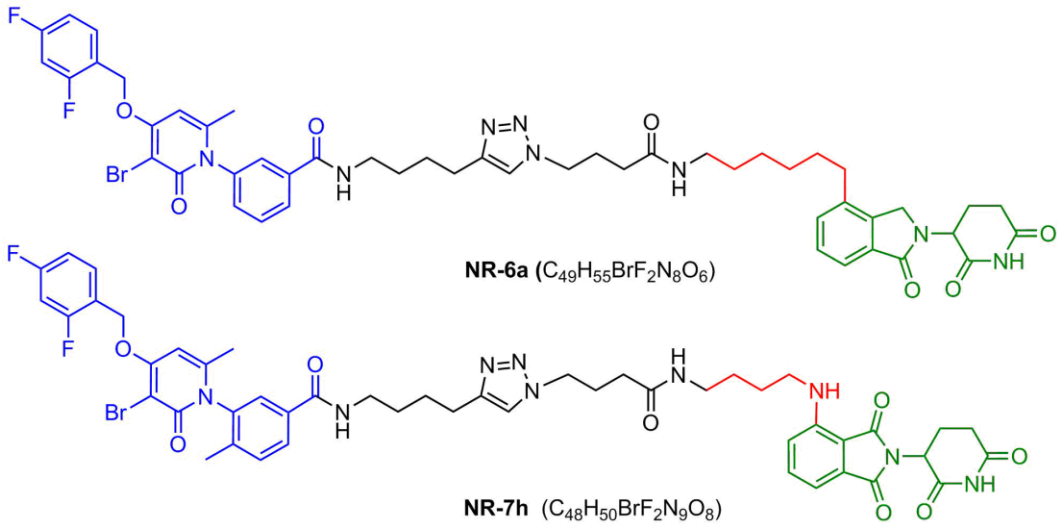

NR-7h in T47D

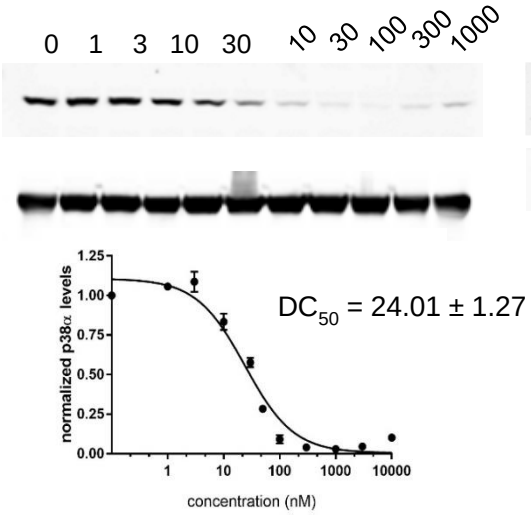

NR-7h in MB-MDA-231

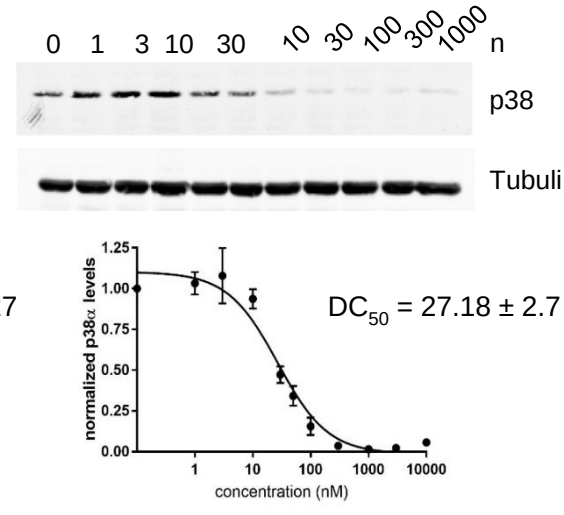

NR-6a in T47D

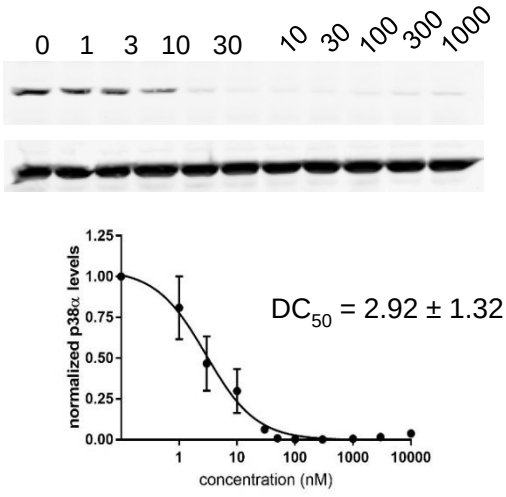

NR-6a in MB-MDA-231

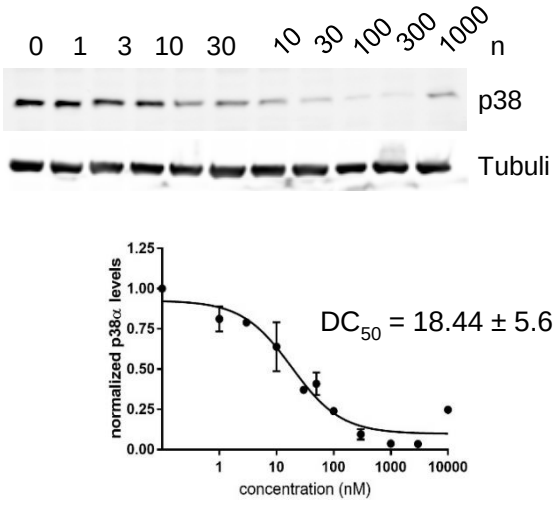

Fig. 4. (a) Chemical structures of the most active PROTACs **NR-6a** and **NR-7h**. (b) Determination of the DC_{50} for p38α degradation. T47D cells and MB-MDA-231 cells were treated with the indicated concentrations of the PROTACs **NR-6a** or **NR-7h** for 24 h, and cell lysates were analyzed by immunoblotting. DC_{50} values were determined based on the quantification of p38α levels in biological duplicates.

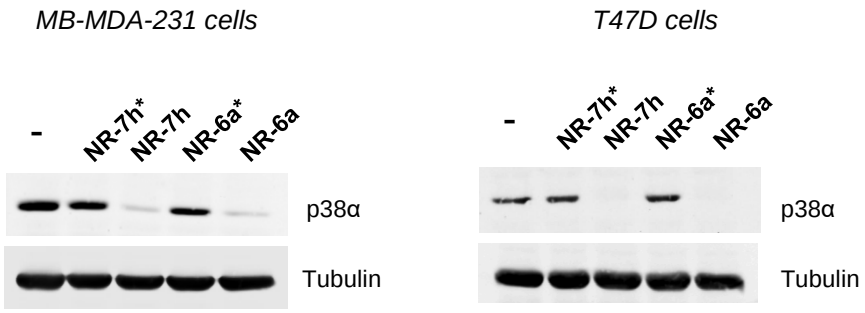

Fig. 5. N-methyl controls did not induce the degradation of p38α and p38β. The indicated cells were treated with 1 μM of **NR-7h** or **NR-6a** or methylated controls **NR-7h*** or **NR-6a*** for 24 h, and then were analyzed by immunoblotting.

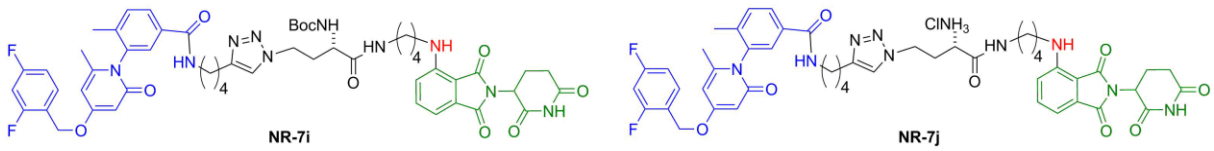

Fig. 6. Structures of compounds **NR-7i** designed to have a protected functionality as derivatization point and **NR-7j** designed to improve solubility.

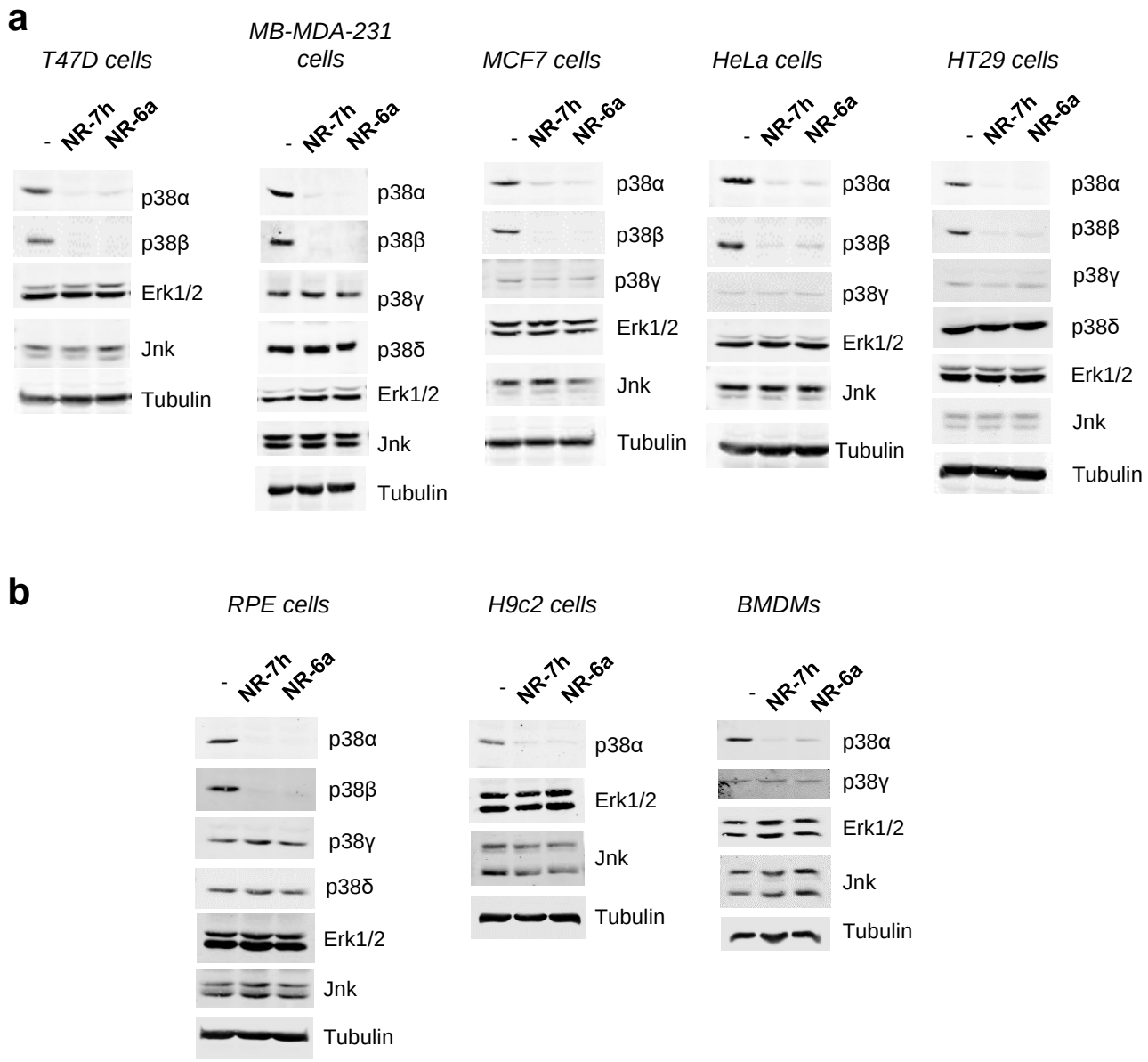

Fig. 7. PROTACs selectively induce the degradation of p38α and p38β but not other MAPKs. (a) The indicated human cancer cell lines were incubated with 1 μM of **NR-7h** or **NR-6a** for 24 h, and then cells lysates were analyzed by immunoblotting. (b) Non-tumoral human retina epithelial cells (RPE), rat cardiomyocytes (H9c2) and mouse bone marrow derived macrophages (BMDMs) were incubated with 1 μM of **NR-7h** or **NR-6a** for 24 h, and then cells lysates were analyzed by immunoblotting.

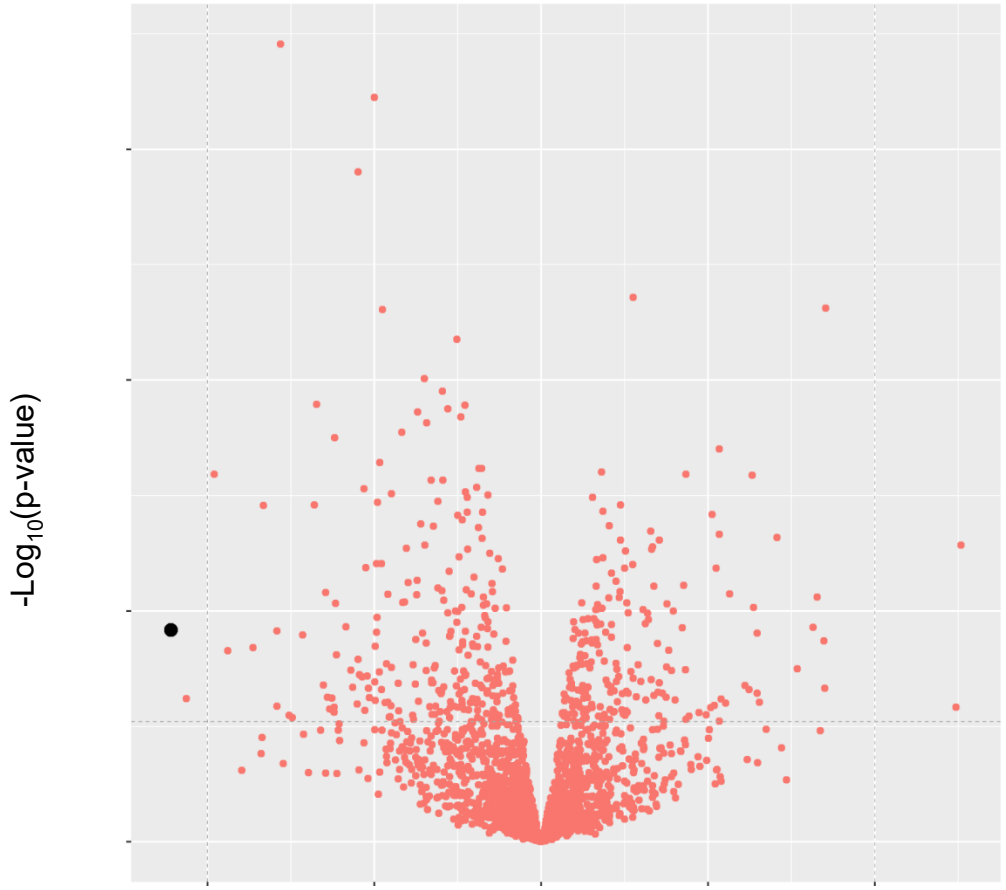

Fig. 8. Proteomic changes in MB-MDA-231 cells treated with 1 μM of **NR-7h** for 16 h. Volcano plot displayed protein abundance (Log_2FC) as a function of significance level (Log_{10}(p-value)).

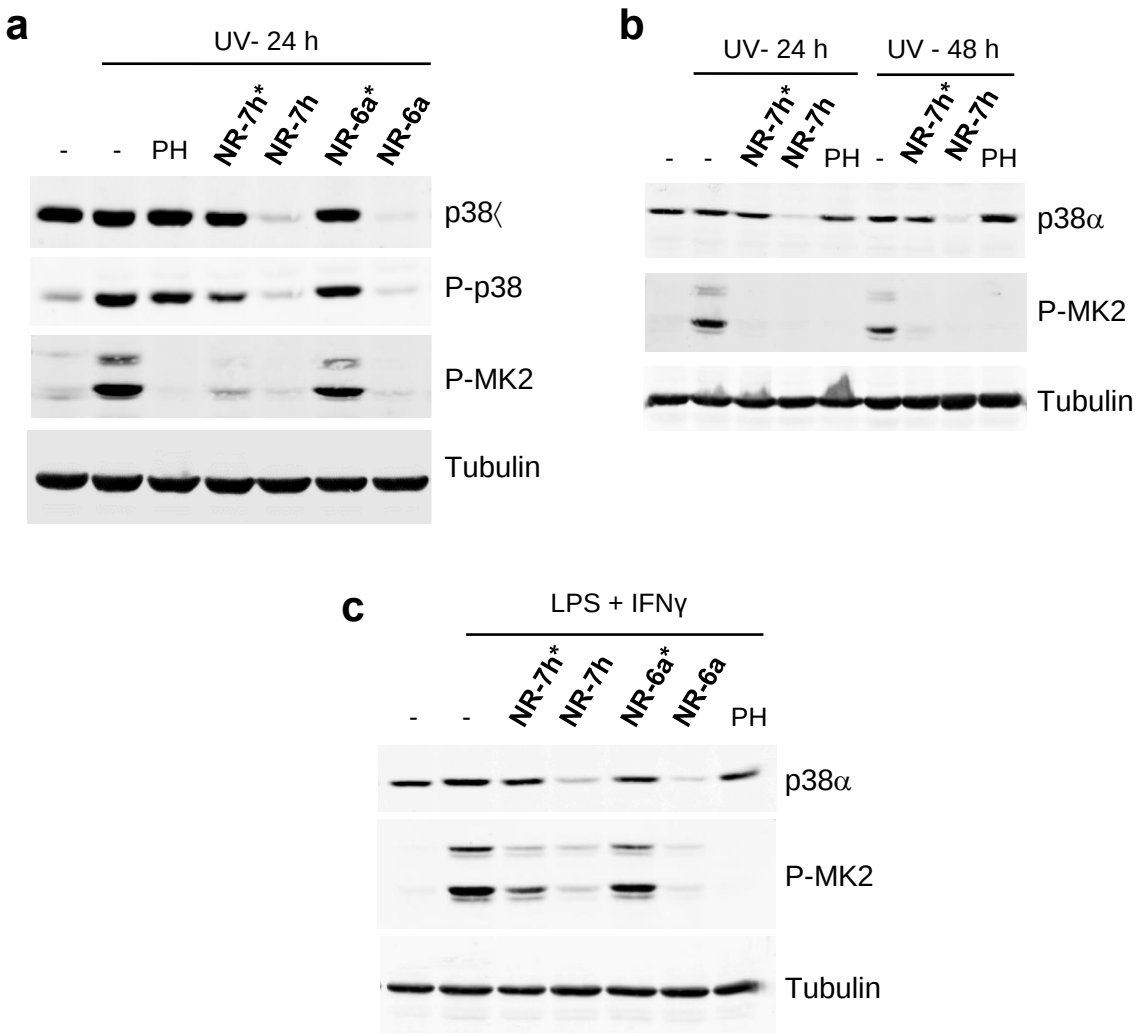

Fig. 9. Inhibition of the p38α pathway by PROTACs in cells. (a and b) MDA-MB-231 cells were treated with 2 μM PH797804 (PH) and 1 μM of **NR-7h, NR-6a** or the N-methyl controls for the indicated times prior to irradiation with UV (30 J/m^2). After 1 h, cells were lysed and analyzed by immunoblotting. (c) BMDMs were pre-treated with DMSO or the indicated compounds at 1 μM for 24 h and then were stimulated with 100 ng/ml LPS and 50 ng/ml IFNγ for 30 min. Cell lysates were collected and analyzed for immunoblotting.